Article | Received 8 November 2025; Revised 12 December 2025; Accepted 28 December 2025; Published 12 January 2026
https://doi.org/10.55092/aic20260001

Optical reconfigurable intelligent surfaces assisted visible light positioning and communications: performance analysis and design optimization

Fasong Wang[1,*], Wen Jiang[1], Rui Li[2], Xingwang Li[3] and Arumugam Nallanathan[4]

[1] School of Electrical and Information Engineering, Zhengzhou University, Zhengzhou 450001, China
[2] School of Mathematics and Statistics, Henan University of Technology, Zhengzhou 450001, China
[3] School of Physics and Electronics Information Engineering, Henan Polytechnic University and the Jiaozuo Key Laboratory of Crow-Sensing Network, Jiaozuo 454003, China
[4] School of Electronic Engineering and Computer Science, Queen Mary University of London, London E1 4NS, UK

* Correspondence author; E-mail: iefswang@zzu.edu.cn.

Highlights:

- ORIS dynamically creates robust non-line-of-sight links to overcome indoor visible light positioning and communication blockage.
- Theoretical bounds (CRLB for positioning, closed-form AMI/BER for OOK communication) establish fundamental performance limits.
- Centimeter-level positioning accuracy and reliable communication are simultaneously achieved under line-of-sight blockage.

Abstract: This paper investigates the integration of visible light positioning and communication (VLP&C) facilitated by optical reconfigurable intelligent surfaces (ORIS) to address line-of-sight (LoS) blockage challenges within indoor environments. In contrast to conventional VLP&C systems, which experience significant performance deterioration under LoS blockage, the proposed ORIS-assisted framework dynamically adjusts the reflection patterns to establish reliable non-LoS (NLoS) links. Initially, a comprehensive system model is formulated, encompassing the physical properties of ORIS, including an analysis of time delays and strategies for ORIS deployment. Subsequently, the Cramér-Rao lower bound (CRLB) for positioning accuracy is rigorously derived from the underlying signal models, thereby providing a realistic theoretical performance benchmark. Additionally, closed-form expression for the average mutual information (AMI) and bit error rate (BER) of the communication subsystem are developed, accounting for the finite-alphabet characteristics of on-off keying (OOK) modulation. The study further investigates the trade-offs between positioning accuracy and communication performance across various system parameters, such as the number of ORIS reflection units, half-power angle, and spatial distribution of users. Extensive simulation results demonstrate that the proposed ORIS-assisted system attains centimeter-level positioning accuracy alongside

reliable communication performance, even in scenarios where LoS links are blocked. The theoretical findings are validated through Monte Carlo simulations, and the practical implementation challenges are discussed to inform future real-world deployments.

Keywords: VLP&C; VLC; CRLB; AMI; ORIS

1. Introduction

The communication and positioning functionalities are fundamental to the development of future sixth-generation (6G) Internet-of-Things (IoT) applications [1]. To accommodate the extensive connections and varied service demands of IoT devices, as well as to address the challenges posed by limited spectrum resources in radio frequency (RF) wireless communication, it is imperative to establish an integrated architecture that combines visible light communication (VLC) and VLP for the creation of a multifunctional 6G wireless networks [2]. However, the majority of existing research on VLC and VLP has been conducted independently [3–6]. In practical scenarios, it may be necessary to implement both communication and positioning services concurrently within the same system of indoor environment [7,8]. Consequently, beyond enhancing the transmission rates and positioning accuracy of the existing systems, it is crucial to explore the feasibility of integrating VLC and VLP into a cohesive system that allows for the simultaneous coexistence of visible positioning and communication signals, or even fosters a collaborative relationship between the two. Research is focused on developing a unified infrastructure that can deliver both positioning and communication capabilities while also fulfilling basic lighting requirements, which holds significant implications for power consumption and cost efficiency [2].

In recent years, VLP has gained significant attention as a promising technology for indoor localization. According to the comprehensive survey by Bastiaens *et al.* [4], VLP offers several advantages over traditional RF-based systems, including higher positioning accuracy, immunity to RF interference, and the ability to leverage existing lighting infrastructure. Furthermore, Zhu *et al.* [9] recently provided an in-depth analysis of indoor VLP systems, highlighting the challenges and opportunities in this field. Their work emphasizes the need for integrated solutions that can simultaneously provide communication and positioning services. In the context of 6G networks, Italiano *et al.* [10] have outlined the evolution from 5G to 6G positioning, identifying VLC as a key enabling technology for ultra-precise indoor localization. These studies collectively indicate that integrated VLP&C systems are an important component of future 6G indoor positioning and communication architectures.

The intricate transmission links of visible light signals within indoor environments pose significant challenges, particularly as the LoS link, which are essential for communication and positioning functions, is prone to blockage. Furthermore, the varying performance and underlying principles of different indoor VLP technologies complicate the development of a universal indoor VLP&C architecture [2]. While NLoS links are more prevalent in indoor settings, the signal strength in visible light NLoS transmission systems-characterized by multiple reflections and diffuse scattering-tends to be considerably weak, thereby adversely affecting the quality of signal transmission.

In this context, optical reconfigurable intelligent surfaces (ORIS) have emerged as a novel optical communication technology. Comprising numerous low-cost passive components, ORIS can modulate the

propagation direction of light beams and other related characteristics, garnering significant attention in recent years [11–17]. Generally, ORIS can be categorized into two types: mirror arrays and metasurfaces [18]. In scenarios where LoS transmission links are blocked or when there is an insufficient number of light emitting diode (LED) transmitters within the indoor wireless networks, reflective transmission links can be established to facilitate auxiliary user positioning and communication functions [19]. This capability renders ORIS a potentially valuable and promising solution for indoor communication and positioning applications [11,12].

It is important to note that unlike conventional diffuse reflections from walls and objects, ORIS can provide controlled specular reflections that are significantly stronger and more directional. This key distinction, as emphasized by Di Renzo *et al.* [14], addresses a fundamental limitation in traditional NLoS VLC systems where diffuse reflections result in weak signal strength and high path loss.

The application of ORIS in indoor VLC and VLP can realize optical power focusing and effectively improve the performance of indoor positioning and communications, so it has been widely studied in their respective application fields [10,20–27]. To be specific, the authors in [23] proposed a low-complexity algorithm to maximize the sum rate of the ORIS-assisted VLC system, and proved that ORIS helps to improve the communication rate of the VLC system and effectively alleviate the blockage problem. Then, in [24], the specular reflection is applied to the indoor VLC system based on space shift keying, and then the orthogonal matching pursuit detection algorithm is proposed for the system, where the effectiveness of the system is verified in the case of LoS link blockage. In addition, research on RIS has also been involved in the field of indoor positioning. The authors in [25] considered a distributed RIS-assisted wireless positioning system and proposes a practical indoor positioning structure, including quasi-static and dynamic modes. In [26], ORIS was integrated into indoor VLP and the joint optimization problem was solved using sparse Bayesian algorithm. Although there are many studies on focusing RIS in wireless positioning algorithms for RF systems [10], the research on ORIS in VLP systems is still under exploration. And because the propagation and reflection characteristics of visible light are very different from those of RF signals, more specific in-depth exploration and research on ORIS-assisted VLP algorithm is needed.

Recent studies have further advanced the understanding of ORIS-assisted systems. Ndjiongue *et al.* [15] provided a comprehensive analysis of the channel characteristics in ORIS-assisted VLC, while Dixit *et al.* [28] demonstrated the potential of ORIS for enhancing positioning accuracy in indoor environments. These works collectively highlight the growing interest in ORIS technology for integrated positioning and communication applications.

Currently, several researchers have investigated VLP&C systems, yielding findings that significantly contribute to the advancement of future research in this domain. The authors in [29] presented an intelligent resource allocation strategy for VLP&C systems, employing reinforcement learning to optimize the system's sum rate, thereby enhancing the quality of service for both communication and positioning. This study primarily concentrates on the optimization of resource allocation across various frequency bands. In [30], a practical adaptive feedback threshold method is implemented within a VLP&C system, which enhances the system's demodulation performance and facilitates the location estimation and effective communication of mobile users through the utilization of multiple photodetectors (PDs). A

VLC scheme that leverages positioning information was presented in [31], by reformulating the robust power allocation challenge for VLP&C systems into a non-convex optimization problem for resolution. However, a significant number of existing studies overlook the blockage issues associated with LoS link in indoor VLP&C systems, and there is a notable deficiency in research concerning ORIS-assisted indoor VLP&C systems.

Drawing inspiration from the application of RIS in RF contexts and the distinctive characteristics of active ORIS, this paper endeavors to integrate positioning and communications systems more closely and to develop a model for an ORIS-assisted indoor VLP&C system. The discussion and analysis focus on an application paradigm that closely resembles real-world scenarios.

In a nutshell, the primary contributions of this paper are delineated as follows:

- An ORIS-assisted indoor VLP&C model is developed to mitigate the LoS link blockage challenges encountered in intricate indoor circumstance, leveraging active ORIS. The proposed system model facilitates the design of an information frame structure that enables the seamless integration of VLP and VLC. This information frame structure is composed of three distinct components: the positioning information frame, the feedback information frame, and the communication information frame.
- Two high-precision three-dimensional positioning methodologies employing ORIS are specifically designed for situations where the user's LoS link is blocked. The first method proposes an indoor dimensionality reduction positioning technique based on the geometric distribution of the user's position in conjunction with ORIS. The second method presents a maximum likelihood positioning approach, predicated on the unique geometric configuration of ORIS. Furthermore, the CRLB for the positioning performance of the ORIS-assisted VLP&C system is derived, providing a theoretical lower bound (LB) for the system's positioning error.
- Employing the proposed system model and the OOK modulation technique, we present an expression for the AMI of the proposed VLP&C system. Additionally, a closed-form solution for its LB is provided, which is derived from the finite-alphabet characteristics of the system's input signal. The simulation analysis encompasses the impact of various system parameters, including the number of ORIS reflective units, half-power angle, and user position distribution, on the performance of both the positioning and communications subsystems. Additionally, the BER performance of the system is also examined.

The subsequent sections of this paper are structured as follows: Section 2 introduces the ORIS-VLP&C integrated system model. Section 3 provides a comprehensive description of the system's design, along with two high-precision positioning algorithms and communication methodologies. Section 4 theoretically analyzes the positioning and communication performance of the proposed VLP&C system. Section 5 presents extensive simulation results. Finally, Section 6 offers a conclusion that encapsulates the findings of the paper.

2. Indoor ORIS-assisted VLP&C system model

2.1. System architecture

VLP&C is fundamentally dependent on the LoS links, as effective data transmission necessitates unblocked links between the transmitter LEDs and receiver PDs [20,21]. Nonetheless, in intricate indoor settings, obstacles that block the visible light propagation can lead to signal blockage, thereby failing to satisfy the requirements for maintaining LoS links in VLP&C. This often results in communication disruptions or a decline in positioning accuracy. To fully harness the capabilities of VLP&C for diverse indoor applications, it is imperative to tackle the issue of LoS link blockage.

In this paper, we examine an integrated indoor VLP&C system enhanced by ORIS to address the issue of LoS signal blockage, thereby enhancing the performance of the VLP&C system. Within the framework of VLP&C systems, the current ORIS are predominantly classified into two categories [12]: passive ORIS, which lack reconfigurability, and active ORIS, which possess reconfigurable capabilities. Passive ORIS operates as reflective devices made from dielectric or metallic substances. The inherent properties of these units remain fixed post-manufacture, precluding dynamic beamforming capabilities and consequently restricting their broader applicability [12]. Conversely, active ORIS comprise intelligent metasurface reflectors or intelligent mirror arrays, which facilitate a reconfigurable wireless propagation environment [20–22].

We consider an indoor VLP&C system consisting of a single LED fixture, an active ORIS, and a user equipment (UE) with a single PD, as illustrated in Figure 1. The LED fixture, typically mounted on the ceiling, serves as the transmitter for both communication and positioning signals. The ORIS, strategically placed on walls or other surfaces, comprises N reconfigurable reflection units that can dynamically adjust their reflection coefficients and angles. The UE, carried by a mobile user, integrates a PD for signal reception and a processing unit for positioning and communication functionality.

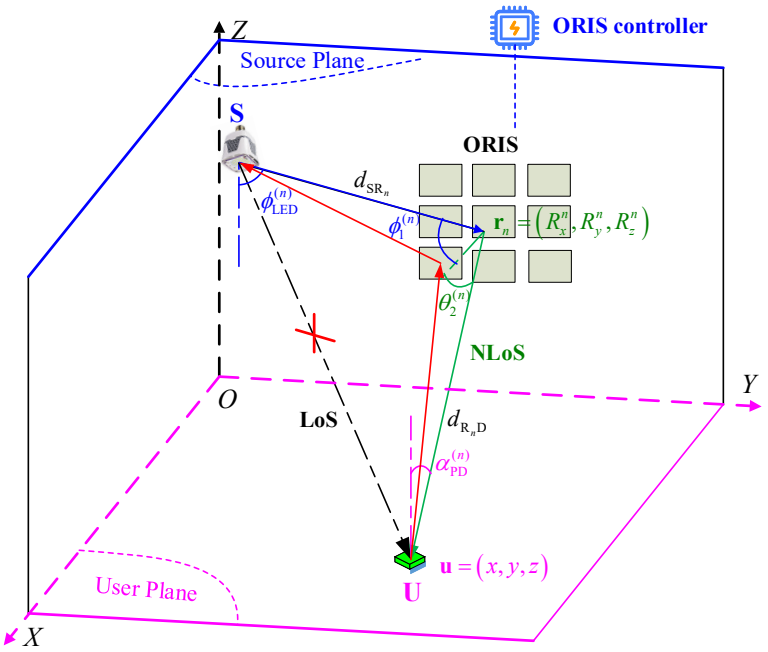

Figure 1. Schematic diagram of the indoor ORIS-assisted VLP&C system.

The considered system operates in two modes: LoS mode when the direct link between the LED and PD is unblocked, and NLoS mode when the LoS link is blocked. In the NLoS mode, the ORIS creates alternative signal paths by reflecting the LED signal to the PD, thereby maintaining both communication connectivity and positioning capability.

To enhance the analytical framework, this study introduces a three-dimensional Cartesian coordinate system to delineate the precise locations of key equipment, as illustrated in Figure 1. The origin O of this coordinate system is established at a corner of the room, with the coordinates of the central position of the nth ORIS reflective unit denoted as $\mathbf{r}_n = (R_x^n, R_y^n, R_z^n)$.

2.2. *ORIS physical characteristics*

Given that the ORIS reflective units are fundamental to the system's architecture, it is assumed that the coordinate positions of all ORIS reflective units are presumed to be predetermined. Additionally, it is proposed that the spatial coordinates of the user to be located are defined as $\mathbf{u} = [x, y, z]^T$. The ORIS is assumed to be square in configuration and composed of $N = L \times L$ multiple reflection units, each with dimensions of $d \times d$, where L represents the total number of rows or columns within the ORIS. The normal vector of each reflection unit can be independently manipulated by the ORIS controller [32].

To concentrate on the NLoS scenario, we assume that the LoS link between the LED and the user PD is blocked, leading to the disruption of the indoor LoS link. Thus, this paper focuses solely on the single reflected path component facilitated by the ORIS, referred to as the NLoS link. It is further assumed that the reflective coefficient of each reflecting unit is identical. It should be highlighted that, aside from the single reflection link, there exist diffuse reflection and scattering components influenced by walls, ceilings, floors, and other objects within ORIS-assisted VLP&C systems. However, the impact of these components is considered negligible in comparison to the channel gains of the NLoS link aided by ORIS [33,34].

Following the aforementioned assumptions and analysis, the channel gain of the ORIS-assisted NLoS link between the LED, the nth reflective unit of the ORIS, and the PD can be represented as [35,36]

$$h_n^{\mathrm{NLoS}} = \begin{cases} \dfrac{\rho \eta \mathscr{T} R A_{\mathrm{r}} A_{\mathrm{Rx}}}{2\pi d_{\mathrm{SR}_n}^2 d_{\mathrm{R}_n\mathrm{D}}^2} (m+1) \cos^m(\phi_{\mathrm{LED}}^{(n)}) & \\ \quad \times \cos\alpha_{\mathrm{PD}}^{(n)} \cos\theta_1^{(n)} \cos\theta_2^{(n)}, & |\alpha_{\mathrm{PD}}^{(n)}| \le \Theta_{\mathrm{FoV}}, \\ 0, & |\alpha_{\mathrm{PD}}^{(n)}| > \Theta_{\mathrm{FoV}}, \end{cases} \tag{1}$$

where ρ denotes the reflectivity of each ORIS reflective unit, satisfies $0 \le \rho \le 1$, representing the fraction of incident optical power that is reflected. d_{SR_n} signifies the distance between the LED transmitter and the nth unit of the ORIS. Additionally, $d_{\mathrm{R}_n\mathrm{D}}$ represents the distance from the nth reflective unit of the ORIS to the PD receiver. Furthermore, A_{r} indicates the reflection area of an individual reflector within the ORIS, the term A_{Rx} refers to the effective receiving area of the PD. $\phi_{\mathrm{LED}}^{(n)}$ represents the angle of irradiance at the LED in relation to the nth ORIS reflective unit, while $\alpha_{\mathrm{PD}}^{(n)}$ denotes the angle of incidence at the PD reflected by the nth ORIS reflective unit. Moreover, $\theta_1^{(n)}$ and $\theta_2^{(n)}$ correspond to the incidence angle and irradiance angle of the optical signal at the nth ORIS reflective unit, respectively, and the Lambertian emission order is represented by $m = -1/\log_2(\cos\Phi_{1/2})$, where $\Phi_{1/2}$ indicates the half-power angle of the LED, while Θ_{FoV} signifies the field of view (FoV) of the PD receiver. Additionally, η represents the

electro-optic conversion efficiency of the LED, $\mathscr{T}$ denotes the gain of the optical filter, and R indicates the responsivity of the PD.

It is important to highlight that, in contrast to traditional diffuse reflection channels, the ORIS-assisted channel provides controlled specular reflections that are significantly stronger than typical diffuse reflections from room surfaces. The specular reflection coefficient ρ of ORIS is typically much higher (e.g., 0.95 as in our simulations) compared to the diffuse reflection coefficients of typical room surfaces (usually below 0.2).

2.3. Time delay analysis

In this subsection, we present a comprehensive analysis of the effects of time delays associated with NLoS paths facilitated by the ORIS on the received signal. Considering the user's spatial coordinates denoted by $\mathbf{u} = [x, y, z]^T$, where the vertical component $z = h_p$ corresponds to the fixed height of the PD, typically set at 1.5 meters for a standard UE in indoor scenarios. The distance between the LED at position $\mathbf{s}_\mathrm{L} = [x_\mathrm{L}, y_\mathrm{L}, z_\mathrm{L}]^T$ and the PD is given by

$$d_\mathrm{SD} = \|\mathbf{u} - \mathbf{s}_\mathrm{L}\|_2, \tag{2}$$

where $\|\cdot\|_2$ denotes the Euclidean norm.

The time delay for the nth reflection NLoS path is given by

$$\tau_n = \frac{d_{\mathrm{SR}_n} + d_{\mathrm{R}_n\mathrm{D}}}{c}, \tag{3}$$

where c is the speed of light.

For typical indoor environments with dimensions of 5 m $\times$ 5 m $\times$ 4 m, the maximum path difference between NLoS paths is approximately 5 m, corresponding to a time delay of

$$\tau_\mathrm{max} = \frac{5}{3 \times 10^8} \approx 16.7 \text{ ns}. \tag{4}$$

The coherence time of visible light signals is typically on the order of microseconds (for modulation bandwidths of hundreds of MHz), which is significantly larger than the maximum time delay. Therefore, the time delay effect can be neglected in the signal model without significant loss of accuracy.

This conclusion holds significant implications for the design of our system, as it: streamlines the signal processing demands; decreases the computational complexity associated with positioning algorithms; and facilitates the implementation of more straightforward frame structures without the need for specialized synchronization techniques.

2.4. Optimal ORIS deployment strategy

Based on the power scaling law analysis in [37], we investigate the optimal deployment of ORIS for integrated VLP&C systems. Unlike RF-based RIS, the performance of ORIS is highly dependent on its geometric position relative to the LED and PD due to the directional nature of visible light propagation.

Let P_ORIS denote the received power at the PD via ORIS reflection, which can be expressed as

$$P_\mathrm{ORIS} \propto \frac{1}{d_\mathrm{SR}^2 + d_\mathrm{RD}^2}, \tag{5}$$

where d_{SR} and d_{RD} are the distances from LED to the center of ORIS and from the center of ORIS to PD, respectively.

To maximize the received power, the ORIS should be positioned such that $d_{SR}^2 + d_{RD}^2$ is minimized for typical user locations. Through geometric analysis, we find that the optimal ORIS position follows the "reflection principle"—the ORIS should be placed such that the angle of incidence equals the angle of reflection with respect to the LED and typical user positions. For a 5 m $\times$ 5 m $\times$ 4 m room with the LED at the center of the ceiling, the optimal positions form a hyperbolic surface where the sum of distances to the LED and typical user locations is constant. For practical implementation, we recommend placing the center of the ORIS on walls at approximately 2.5 m height, which balances coverage area and signal strength.

Having established the comprehensive system model for the ORIS-assisted VLP&C framework, we now proceed to the detailed design of the integrated system.

3. Integrated design of the ORIS-assisted VLP&C system

The integrated realization of the ORIS-assisted VLP&C system is achieved through the design of an information frame structure, which comprises three fundamental components: the positioning information frame, the feedback information frame, and the communication information frame. Each of these components will be analyzed individually in the subsequent sections.

3.1. Positioning information frame

This study employs an active ORIS [38] configured in a square arrangement. During the positioning phase, we propose two approaches: (1) a selective activation strategy where only the four corner reflective units are activated to minimize interference while ensuring sufficient spatial diversity, and (2) a full activation strategy where all ORIS elements are simultaneously activated with different phase shifts for improved signal-to-noise ratio (SNR) and positioning accuracy.

The selective activation strategy is particularly useful in scenarios with limited processing capabilities or when the system needs to minimize interference with communication signals. We note that while activating all ORIS elements would provide better positioning accuracy due to the increased number of measurements and improved SNR, it also introduces several practical challenges: increased interference between signals from different elements, higher computational complexity for signal processing, and potential for correlated measurements that don't provide independent information. This study primarily emphasizes the selective activation strategy due to its simplicity and practical feasibility. Nonetheless, it is recognized that systems endowed with adequate processing capabilities may achieve further performance improvements by activating a greater number of elements with optimally designed phase shifts. This avenue constitutes a promising direction for future research.

To achieve robust positioning in dynamic indoor environments, the proposed framework adopts received signal strength (RSS)-based geometric measurement. Compared to angle- or time-based methods, RSS positioning avoids the need for high-resolution angular detection (as in angle of arrival (AOA) triangulation) or strict clock synchronization (required by time of arrival (TOA)/time difference of arrival (TDOA)) [9,39]. Its simplicity and low complexity make it ideal for practical ORIS-aided systems.

In response to the aforementioned analysis, this study presents two VLP algorithms aimed at alleviating the coplanar effects associated with the reference point in indoor settings, employing ORIS and based on the RSS positioning technique of geometric measurement.

It is posited that the reflectivity of the ORIS remains stable over an extended temporal framework, with the simultaneous activation of four reflective units from a total of N units within the ORIS system, if the positioning optical signal emitted from the transmitter LED is denoted by $s_{\mathrm{p}}(t)$, the received signal obtained at the PD of the user by reflection from the nth reflective unit of ORIS can be expressed as

$$y_{\mathrm{p},n}(t) = h_{\mathrm{p},n} s_{\mathrm{p}}(t-\tau_n) + n_{\mathrm{p}}(t), \tag{6}$$

where the subscript 'p' denotes the signal associated with positioning frame, $h_{\mathrm{p},n}$ represents the VLC channel gain between the LED and the PD of the UE aided by the nth ORIS reflective unit, which can be derived from Equation (1). Additionally, $n_{\mathrm{p}}(t)$ is characterized as zero-mean additive white Gaussian noise (AWGN) processes with variance of σ_{p}^2 . Furthermore, τ_n denotes the signal delay from the LED, through the nth ORIS reflective unit, to the receiving PD, which is calculated by

$$\tau_n = \frac{d_{\mathrm{SR}_n} + d_{\mathrm{R}_n\mathrm{D}}}{c}. \tag{7}$$

Based on this signal model, the log-likelihood function for the received signal can be derived as

$$\ln f\left(y_{\mathrm{p},n}(t) \mid \tau_n\right) = l_n - \frac{1}{2\sigma_{\mathrm{p}}^2} \times \int_0^{T_{\mathrm{p}}} \left[y_{\mathrm{p},n}(t) - h_{\mathrm{p},n} s_{\mathrm{p}}(t-\tau_n)\right]^2 \mathrm{d}t. \tag{8}$$

where l_n is a constant independent of the unknown parameter τ_n, and T_{p} is the observation time of the positioning signal. Then the estimated value of the corresponding delay τ_n can be expressed as

$$\hat{\tau}_n = \arg\max_{\tau_n} \int_0^{T_{\mathrm{p}}} y_{\mathrm{p},n}(t) s_{\mathrm{p}}\left(t-\tau_n\right) \mathrm{d}t. \tag{9}$$

In the context of the positioning information frame, the locations of the LED transmitter and the ORIS reflective units are predetermined and remain constant, resulting in a quasi-static channel between the LED and the ORIS, and the distance d_{SR_n} can be calculated directly. Furthermore, the instantaneous nature of the reflection from the ORIS ensures that it does not contribute to an increase in the total arrival time, as referenced in [40]. Consequently, τ_n can be estimated using Equation (9). Once $\hat{\tau}_n$ is determined, the estimated value $\hat{d}_{\mathrm{R}_n\mathrm{D}}$ of distance $d_{\mathrm{R}_n\mathrm{D}}$ can be derived according to Equation (7).

The subsequent focus of this section is on how to utilize $\hat{d}_{\mathrm{R}_n\mathrm{D}}$ to ascertain the location information of the user for positioning. Specifically, the VLP receiver independently extracts the received signal $y_{\mathrm{p},n}(t)$ from each ORIS reflective unit, employing various positioning methodologies to deduce the user's positional information. This paper introduces two RSS-based VLP techniques within the ORIS framework. It is important to highlight that a manageable signal model is achieved by disregarding the multipath component, which facilitates theoretical analysis and provides an intuitive understanding of the influence of ORIS on VLP&C systems.

3.1.1. Three-dimensional two-step dimensionality reduction positioning algorithm

To determine the three-dimensional coordinates information of the user being positioned, this section initially employs a three-dimensional two-step dimensionality reduction positioning (2SDRP) technique based on RSS. This approach reformulates the three-dimensional positioning challenge, facilitated by an ORIS, into a superposition problem involving multiple parallel two-dimensional planes within the third dimension. These parallel planes are situated in the space between the plane containing the ORIS and the plane housing the PD receiver of the user under examination, which is oriented parallel to the ORIS plane. It is important to note that the position of the ORIS reflective unit is predetermined within the ORIS-assisted localization framework, and the intervals perpendicular to the reflection plane must be stratified at the onset of the localization process.

As illustrated in Figure 1, the system model addressed in this paper consists of planes that are parallel to the YOZ plane, extending in the positive direction along the X-axis. It is assumed that the thickness of each layer is limited between the minimum value $x_{\min}$ of X-axis coordinate (the X-axis coordinate of ORIS) and the maximum value $x_{\max}$ of X-axis coordinate (the maximum value of user's possible X-axis coordinate), and the resolution of each layer is Δx. Consequently, the distance calculation equation of $d_{\mathrm{R}_n\mathrm{D}}$ can be reformulated into a circular representation equation, allowing for the extraction of distance information through the computation of the overlapping area of each circle.

This iterative process is conducted multiple times to enhance positioning accuracy, ultimately identifying the estimated value $\hat{x}$ of the user's X-axis coordinate x at the point of minimal overlap area. Algorithm 1 delineates the procedural flow of the ORIS-assisted three-dimensional 2SDRP algorithm.

Algorithm 1 ORIS-assisted three-dimensional 2SDRP VLP algorithm.

Input: The estimate $\hat{d}_{\mathrm{R}_n\mathrm{D}}$ of $d_{\mathrm{R}_n\mathrm{D}}$.

Output: The estimated value $\hat{x}$ of the X-coordinate of the user located.

1: Initialization: Minimum area value $S_{\min}$.
2: **for** $x = x_{\min} : \Delta x : x_{\max}$ **do**
3: Determine the distance $|\tilde{r}_n|$ between the projection of the nth ORIS reflective unit onto the plane of the corresponding layer with X-coordinate of x, which is defined by the user's location represented by $\tilde{r}_n^2 = \hat{d}_{\mathrm{R}_n\mathrm{D}}^2 - (x - R_x^n)^2$, $n = 1,2,3,4$.
4: In the plane corresponding to the layer of x, a circle is constructed with its center at the projection of the center of the nth ORIS reflective unit and a radius equal to $|\tilde{r}_n|$, as determined by $\tilde{r}_n^2 = (y - R_y^n) - (z - R_z^n)^2$. The intersection points and the overlapping area $S(x)$ resulting from the pairwise combinations are subsequently calculated, $n = 1,2,3,4$.
5: **if** $S(x) < S_{\min}$ **then**
6: $S_{\min} = S(x)$; $\hat{x} = x$.
7: **end if**
8: **end for**

By employing the obtained estimate $\hat{x}$, the subsequent equations can be given by

$$\hat{d}_{\mathrm{R}_1\mathrm{D}}^2 = (\hat{x} - R_x^1)^2 + (y - R_y^1)^2 + (z - R_z^1)^2, \tag{10}$$

$$\hat{d}^2_{\mathrm{R_2D}} = (\hat{x} - R^2_x)^2 + (y - R^2_y)^2 + (z - R^2_z)^2, \tag{11}$$

$$\hat{d}^2_{\mathrm{R_3D}} = (\hat{x} - R^3_x)^2 + (y - R^3_y)^2 + (z - R^3_z)^2, \tag{12}$$

$$\hat{d}^2_{\mathrm{R_4D}} = (\hat{x} - R^4_x)^2 + (y - R^4_y)^2 + (z - R^4_z)^2. \tag{13}$$

The user's estimated location, denoted as $\hat{\mathbf{u}} = (\hat{x}, \hat{y}, \hat{z})$, can be determined by applying the least-squares method to solve Equations (10)–(13). This process involves subtracting Equation (13) from Equations (10), (11), and (12), individually, and subsequently formulating

$$K_i = (\hat{x} - R^4_x)^2 - (\hat{x} - R^i_x)^2 - (R^4_y - R^i_y)^2 - (R^4_z - R^i_z)^2, \quad i = 1, 2, 3. \tag{14}$$

Upon completion, the following equation is derived

$$\mathbf{Bp} = \mathbf{g}, \tag{15}$$

where

$$\mathbf{B} = \begin{bmatrix} R^4_y - R^1_y & R^4_z - R^1_z \\ R^4_y - R^2_y & R^4_z - R^2_z \\ R^4_y - R^3_y & R^4_z - R^3_z \end{bmatrix}, \tag{16}$$

$$\mathbf{p} = [y \;\; z]^T, \tag{17}$$

$$\mathbf{g} = \frac{1}{2} \begin{bmatrix} d^2_{\mathrm{R_1D}} - d^2_{\mathrm{R_4D}} + K_1 \\ d^2_{\mathrm{R_2D}} - d^2_{\mathrm{R_4D}} + K_2 \\ d^2_{\mathrm{R_3D}} - d^2_{\mathrm{R_4D}} + K_3 \end{bmatrix}. \tag{18}$$

The least-squares solution is given by

$$\mathbf{p} = (\mathbf{B}^T \mathbf{B})^{-1} \mathbf{B}^T \mathbf{g}. \tag{19}$$

In summary, the three-dimensional 2SDRP algorithm utilizing ORIS provides a methodology for achieving precise positioning through the repeated computation of the overlapping area between parallel circles.

3.1.2. Maximum likelihood positioning algorithm

As previously indicated, it is posited that, for a specific ORIS, only the reflection units located at the four corners of the reflecting surface are engaged. The central coordinates of these four reflection units are designated as $\mathbf{r}_1 = (0, a, b)$, $\mathbf{r}_2 = (0, c, b)$, $\mathbf{r}_3 = (0, c, q)$, and $\mathbf{r}_4 = (0, a, q)$, respectively, where a, b, c, and d represent real numbers, as illustrated in Figure 2. Referring to Figure 2, the actual distances from the reflection units situated at the four corners of the ORIS to the user receiver PD can be formulated as

$$\begin{cases} d_{\mathrm{R_1D}} = \sqrt{x^2 + (y-a)^2 + (z-b)^2}, \\ d_{\mathrm{R_2D}} = \sqrt{x^2 + (y-c)^2 + (z-b)^2}, \\ d_{\mathrm{R_3D}} = \sqrt{x^2 + (y-c)^2 + (z-q)^2}, \\ d_{\mathrm{R_4D}} = \sqrt{x^2 + (y-a)^2 + (z-q)^2}. \end{cases} \tag{20}$$

In accordance with the maximum likelihood criterion, determining the user's location information $\mathbf{u} = (x, y, z)$ from the estimated distance $\hat{d}_{\mathrm{R}_n\mathrm{D}}(n = 1, 2, 3, 4)$ necessitates the minimization of the objective function $J = \sum_{n=1}^{4}(d_{\mathrm{R}_n\mathrm{D}} - \hat{d}_{\mathrm{R}_n\mathrm{D}})^2$. To derive its closed-form solution, it is necessary to equate the partial derivatives of the objective function with respect to the variables x, y, and z to zero. This leads to the respective expressions for the solution as

$$\frac{\partial J}{\partial x} = \sum_{n=1}^{4} \frac{2x(d_{\mathrm{R}_n\mathrm{D}} - \hat{d}_{\mathrm{R}_n\mathrm{D}})}{d_{\mathrm{R}_n\mathrm{D}}} = 0, \tag{21}$$

$$\frac{\partial J}{\partial y} = \sum_{n=1}^{4} \frac{2y(d_{\mathrm{R}_n\mathrm{D}} - \hat{d}_{\mathrm{R}_n\mathrm{D}})}{d_{\mathrm{R}_n\mathrm{D}}} - \sum_{n=2,3} \frac{2c(d_{\mathrm{R}_n\mathrm{D}} - \hat{d}_{\mathrm{R}_n\mathrm{D}})}{d_{\mathrm{R}_n\mathrm{D}}} - \sum_{n=1,4} \frac{2a(d_{\mathrm{R}_n\mathrm{D}} - \hat{d}_{\mathrm{R}_n\mathrm{D}})}{d_{\mathrm{R}_n\mathrm{D}}} = 0, \tag{22}$$

$$\frac{\partial J}{\partial z} = \sum_{n=1}^{4} \frac{2z(d_{\mathrm{R}_n\mathrm{D}} - \hat{d}_{\mathrm{R}_n\mathrm{D}})}{d_{\mathrm{R}_n\mathrm{D}}} - \sum_{n=1,2} \frac{2b(d_{\mathrm{R}_n\mathrm{D}} - \hat{d}_{\mathrm{R}_n\mathrm{D}})}{d_{\mathrm{R}_n\mathrm{D}}} - \sum_{n=3,4} \frac{2q(d_{\mathrm{R}_n\mathrm{D}} - \hat{d}_{\mathrm{R}_n\mathrm{D}})}{d_{\mathrm{R}_n\mathrm{D}}} = 0. \tag{23}$$

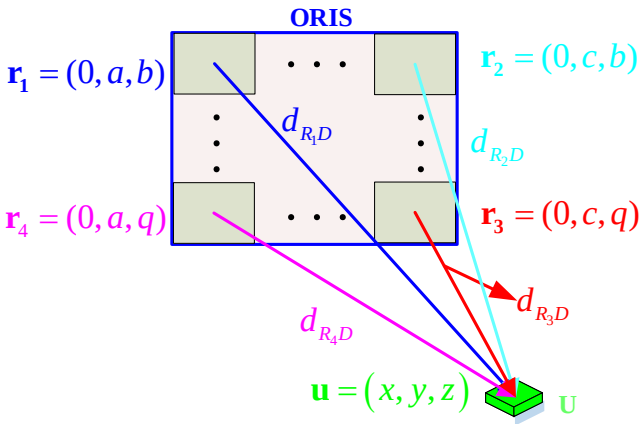

Figure 2. Model diagram of the maximum likelihood positioning algorithm for the ORIS-assisted VLP&C system.

By simplifying Equations (21), (22) and (23), and substituting $d_{\mathrm{R}_1\mathrm{D}}$ for $d_{\mathrm{R}_2\mathrm{D}}$, $d_{\mathrm{R}_3\mathrm{D}}$, and $d_{\mathrm{R}_4\mathrm{D}}$, the resulting expression can be represented as

$$d_{\mathrm{R}_2\mathrm{D}} = \frac{\hat{d}_{\mathrm{R}_2\mathrm{D}} d_{\mathrm{R}_1\mathrm{D}}}{2d_{\mathrm{R}_1\mathrm{D}} - \hat{d}_{\mathrm{R}_1\mathrm{D}}}, \tag{24}$$

$$d_{\mathrm{R}_3\mathrm{D}} = \frac{\hat{d}_{\mathrm{R}_3\mathrm{D}} d_{\mathrm{R}_1\mathrm{D}}}{d_{\mathrm{R}_1\mathrm{D}}}, \tag{25}$$

$$d_{\mathrm{R}_4\mathrm{D}} = \frac{\hat{d}_{\mathrm{R}_4\mathrm{D}} d_{\mathrm{R}_1\mathrm{D}}}{2d_{\mathrm{R}_1\mathrm{D}} - \hat{d}_{\mathrm{R}_1\mathrm{D}}}. \tag{26}$$

Given that the designed ORIS plane is rectangular, then we have $d_{\mathrm{R}_1\mathrm{D}}^2 + d_{\mathrm{R}_3\mathrm{D}}^2 - d_{\mathrm{R}_2\mathrm{D}}^2 - d_{\mathrm{R}_4\mathrm{D}}^2 = 0$, so $d_{\mathrm{R}_1\mathrm{D}}$ can be formulated as

$$d_{\mathrm{R}_1\mathrm{D}} = \frac{\hat{d}_{\mathrm{R}_1\mathrm{D}}(\hat{d}_{\mathrm{R}_1\mathrm{D}}^2 + \hat{d}_{\mathrm{R}_2\mathrm{D}}^2 \pm \mathscr{D})}{2(\hat{d}_{\mathrm{R}_1\mathrm{D}}^2 + \hat{d}_{\mathrm{R}_3\mathrm{D}}^2)}, \tag{27}$$

where $\mathscr{D} = \sqrt{(\hat{d}_{\mathrm{R}_1\mathrm{D}}^2 + \hat{d}_{\mathrm{R}_3\mathrm{D}}^2)(\hat{d}_{\mathrm{R}_2\mathrm{D}}^2 + \hat{d}_{\mathrm{R}_4\mathrm{D}}^2)}$.

From Equation (27), it can be inferred that at least one root of the variable $d_{\mathrm{R_1D}}$ is a positive real number. The appropriate solution can be determined as follows: if there exists only one positive root, this root is designated as the final value of $d_{\mathrm{R_1D}}$. Alternatively, if multiple roots are positive, the solution associated with the minimum value of the objective function is selected as the final value of $d_{\mathrm{R_1D}}$.

Furthermore, it is important to acknowledge that the aforementioned condition $d_{\mathrm{R_1D}}^2 + d_{\mathrm{R_3D}}^2 - d_{\mathrm{R_2D}}^2 - d_{\mathrm{R_4D}}^2 = 0$ is applicable solely under the premise that the four activated ORIS reflective unit reference points must reside on a common plane and constitute rectangles, specifically those that are diagonally bisected and congruent. In contrast, the three-dimensional 2SDRP algorithm proposed earlier in this section does not impose analogous constraints on the topological structure of the ORIS reflective units. Instead, the topological configuration influences the accuracy of positioning in 2SDRP algorithm, rather than determining the feasibility of the positioning function itself.

As illustrated in Figure 2, when the user's position is established in front of the ORIS, specifically in the positive direction of the X-axis, the default value of parameter $\hat{x}$ is greater than zero. Consequently, based on Equations (24)–(27) and the principles of Euclidean geometry, the the user's coordinates are ultimately determined by

$$\hat{y} = \frac{d_{\mathrm{R_1D}}^2 - d_{\mathrm{R_2D}}^2 - d_{\mathrm{R_3D}}^2 + d_{\mathrm{R_4D}}^2 - 2(a^2 - c^2)}{4(c-a)}, \tag{28}$$

$$\hat{z} = \frac{d_{\mathrm{R_1D}}^2 + d_{\mathrm{R_2D}}^2 - d_{\mathrm{R_3D}}^2 - d_{\mathrm{R_4D}}^2 - 2(b^2 - q^2)}{4(q-b)}, \tag{29}$$

$$\hat{x} = \sqrt{d_{\mathrm{R}_n\mathrm{D}}^2 - (\hat{y} - R_y^n)^2 - (\hat{z} - R_z^n)^2}, \quad n \in \{1,2,3,4\}. \tag{30}$$

The positioning information frame provides the foundation for user location estimation, which is essential for subsequent communication optimization. Building upon this positioning capability, the feedback information frame enables the transmission of location information back to the central controller, facilitating adaptive system configuration.

3.2. Feedback information frame

In the feedback information frame, the receiver forwards the user's estimated location coordinates, denoted as $\hat{\mathbf{u}} = [\hat{x}, \hat{y}, \hat{z}]^T$, to the central controller[1] through the infrared (IR) feedback channel, while maintaining fixed orientations of both the LED transmitter and the PD receiver.

The IR feedback channel operates in 850–940 nm wavelength range, strategically selected to avoid spectral overlap with VLC signals (typically 400–700 nm). This specific wavelength choice at 850 nm offers four significant advantages: Immunity to electromagnetic interference from coexisting wireless systems operating in RF bands; Inherent physical layer security through LoS confinement; Availability of cost-effective, commercially mature IR transceiver components that facilitate seamless integration with existing VLC infrastructure; Compliance with eye-safe irradiance limits. Based on Equation (1), the

[1] The central controller is a critical component of the ORIS-assisted VLP&C system, serving as the coordination hub for all system elements. It typically consists of: an embedded processing unit, ORIS control interface for configuring reflection patterns, LED driver circuitry for signal transmission control, infrared receiver for feedback information, and network interface for integration with building management systems.

estimated channel gain between the LED transmitter and PD receiver can be formulated as

$$\hat{h}_{c,n} = \frac{\rho \eta \mathscr{T} R A_r A_{Rx}}{2\pi d_{SR_n}^2 \hat{d}_{R_nD}^2} (m+1) \cos^m(\phi_{LED}^{(n)}) \times \cos \hat{\alpha}_{PD}^{(n)} \cos \theta_1^{(n)} \cos \hat{\theta}_2^{(n)}, \tag{31}$$

where the subscript 'c' denotes the information associated with communication frame, $\hat{d}_{R_nD} = \|\mathbf{r}_n - \hat{\mathbf{u}}\|_2$ represents the estimated distance between the nth unit of the ORIS and the user receiver PD, with $n = 1,2,3,4$ indexing the representative reflective elements analyzed in this context. The parameters $\hat{\theta}_2^{(n)}$ and $\hat{\alpha}_{PD}^{(n)}$ denote the estimated angle of irradiate from the nth ORIS unit to the PD receiver and the corresponding estimated angle of incidence at the PD, respectively. All remaining parameters maintain identical definitions to those established in Equation (1).

Based on the Cartesian coordinates of the reflecting point and the estimated user position, for $n = 1,2,3,4$, the irradiate angle $\hat{\theta}_2^{(n)}$ and incidence angle $\hat{\alpha}_{PD}^{(n)}$ are derived through spherical coordinate transformation as

$$\hat{\theta}_2^{(n)} = \arcsin\left(\frac{|R_x^n - \hat{x}|}{\hat{d}_{R_nD}}\right), \tag{32}$$

$$\hat{\alpha}_{PD}^{(n)} = \arcsin\left(\frac{|R_z^n - \hat{z}|}{\hat{d}_{R_nD}}\right). \tag{33}$$

With respect to user alignment requirements, the proposed architecture implements a wide-FoV IR receiver (120° FoV) at the central controller, which fundamentally mitigates orientation sensitivity without requiring mechanical tracking mechanisms. Additionally, it can effectively eliminating the need for precise user alignment in indoor environments.

We then quantitatively characterizes the relationship between receiver FoV and feedback transmission reliability in indoor IR communication systems through a rigorous simulation framework compliant with IEEE 802.15.7-2011 standards [41]. The Monte Carlo methodology employed 10000 orientation samples per FoV point, ensuring statistical significance with a 95% confidence interval and ±1.5% margin of error. The channel model incorporates the standard Lambertian radiation pattern [42] with order $m = 1$, representing diffuse transmission from handheld devices. Critical physical layer parameters were calibrated against empirical measurements from commercial infrared systems [43]: transmit power of 26 mW, communication distance of 2.3 m, receiver specifications featuring a 2.0 cm diameter photodiode with 0.6 A/W responsivity, and comprehensive noise modeling including shot noise and thermal noise components per IEEE 802.15.7 Section 6.3.2 [44]. The success criterion was defined as SNR $\geq$ 7 dB, sufficient for QPSK modulation at BER $= 10^{-3}$ under typical indoor ambient conditions ($\leq$100 lux). User orientation variations were modeled in accordance with yaw angles uniformly distributed in $[-60°, 60°]$ and pitch angles in $[-30°, 30°]$.

As demonstrated in Figure 3, the results reveal a nonlinear relationship between FoV and reliability, with a critical threshold at 114° FoV where reliability exceeds the 95% benchmark required for robust system operation. At the designed 120° FoV with 26 mW transmit power, the system achieves 99.2% reliability, validating the effectiveness of wide FoV receivers in eliminating precise alignment requirements.

The reliability curve exhibits characteristic saturation behavior beyond 120° FoV. This phenomenon aligns with theoretical analysis of the Lambertian channel model [42], where increased FoV admits additional background radiation noise while providing diminishing signal capture benefits.

With respect to feedback channel imperfections, the current model assumes ideal feedback conditions as a standard simplifying assumption in initial system analysis. While practical implementations may experience erroneous feedback links, such imperfections introduce additional channel estimation error that degrades state information accuracy. As demonstrated in the alignment analysis above, the wide FoV receiver design provides inherent robustness against orientation-related channel variations. However, quantifying the performance degradation under realistic feedback error conditions—including both channel estimation errors and potential packet loss—constitutes a critical direction for future research, particularly when analyzing system performance under practical deployment scenarios.

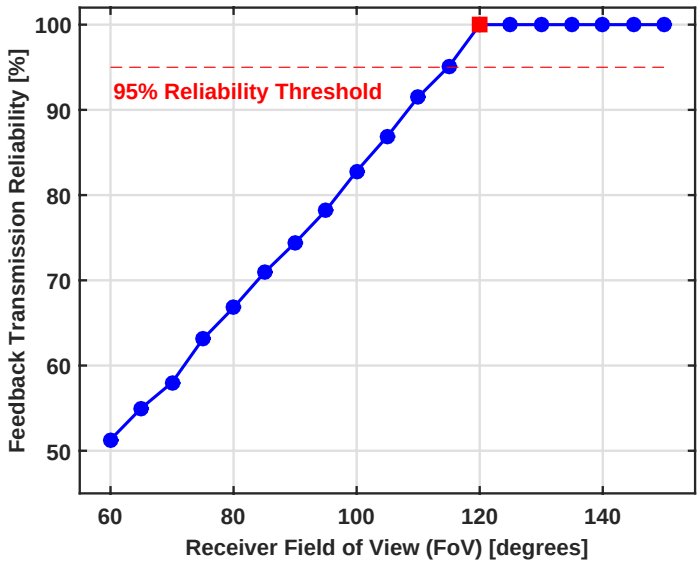

Figure 3. Relationship between feedback transmission reliability and receiver FoV of the ORIS-assisted VLP&C system.

3.3. Communication information frame

In the VLP&C system framework assisted by ORIS, we employ the OOK modulation for data modulation and data transmission. This binary modulation scheme, widely adopted in VLC systems, encodes information by modulating the LED intensity between two levels corresponding to binary symbols 0 and 1, with equal prior probability $p(0) = p(1) = 0.5$.

The LED transmitted signal must satisfy fundamental VLC constraints: non-negativity of optical intensity and average optical power limitations. Specifically, the instantaneous optical power $s(t)$ must satisfy $s(t) \geq 0$ for all t, with the average optical power constrained by $\mathbb{E}[s(t)] = \xi P_{\text{total}}$, where $\xi \in (0, 1]$ represents the dimming target and P_{total} denotes the total available optical power. Let $\tilde{s}$ denote the optical power level allocated for communication signals, constrained such that $\tilde{s} = P_{\text{c}}$ where P_{c} represents the communication power budget, and $x_{\text{ook}}(t) \in \{0, 1\}$ is the normalized OOK symbol with $\mathbb{E}[x_{\text{ook}}(t)] = 0.5$ for equiprobable binary symbols. Then $s(t) = \tilde{s} x_{\text{ook}}(t)$.

Following channel state information (CSI) acquisition through the positioning frame and feedback mechanism, the communication signal $y_{\text{c}}(t)$ received at the user's PD can be expressed as

$$y_{\mathrm{c}}(t) = \sum_{n=1}^{N} h_{\mathrm{c},n} s(t) + n_{\mathrm{c}}(t), \tag{34}$$

where $n_{\mathrm{c}}(t)$ represents zero-mean AWGN with variance σ_{c}^2. This signal model ensures compliance with both the non-negativity constraint ($s(t) \geq 0$) and the average power constraint ($\mathbb{E}[\tilde{s}x_{\mathrm{ook}}(t)] = 0.5\tilde{s} \leq \xi P_{\mathrm{total}}$), which are fundamental requirements for practical VLC implementations.

The integrated nature of VLP&C systems creates a fundamental interdependence between positioning accuracy and communication performance, which directly impacts the BER of the system. This coupling arises because the CSI used for communication signal processing is derived from the estimated user position, making communication performance inherently dependent on positioning accuracy.

Specifically, let $\mathbf{u}$ and $\hat{\mathbf{u}}$ denote the true and estimated user positions, respectively, with positioning error $\varepsilon_p = \|\mathbf{u} - \hat{\mathbf{u}}\|_2$. The channel gain estimation error $\Delta h_{\mathrm{c},n}$ resulting from this positioning error can be rigorously expressed using the mean value theorem for multivariable functions

$$\Delta h_{\mathrm{c},n} = h_{\mathrm{c},n}(\mathbf{u}) - h_{\mathrm{c},n}(\hat{\mathbf{u}}) \approx \nabla^T h_{\mathrm{c},n}(\mathbf{u}^*)(\mathbf{u} - \hat{\mathbf{u}}), \tag{35}$$

where $\mathbf{u}^*$ is a point on the line segment connecting $\mathbf{u}$ and $\hat{\mathbf{u}}$, and $\nabla h(\mathbf{u}^*)$ represents the gradient of the channel gain with respect to user position. This relationship establishes the upper bound

$$|\Delta h_{\mathrm{c},n}| \leq \|\nabla h_{\mathrm{c},n}(\mathbf{u}^*)\|_2 \cdot \varepsilon_p, \tag{36}$$

demonstrating that channel estimation error grows linearly with positioning error, scaled by the spatial rate of change of the channel.

For the OOK modulation employed in our system, the received SNR is proportional to $h_{\mathrm{c},n}^2$. When the communication system operates with imperfect CSI due to positioning errors, the effective SNR becomes

$$\begin{aligned} \gamma_{\mathrm{eff}} &= \frac{\left(\sum_{n=1}^{N} (h_{\mathrm{c},n} + \Delta h_{\mathrm{c},n})\right)^2 P_{\mathrm{c}}}{\sigma_{\mathrm{c}}^2} \\ &= \gamma_0 \left(1 + \frac{\sum_{n=1}^{N} \Delta h_{\mathrm{c},n}}{\sum_{n=1}^{N} h_{\mathrm{c},n}}\right)^2, \end{aligned} \tag{37}$$

where $\gamma_0 = \frac{\left(\sum_{n=1}^{N} h_{\mathrm{c},n}\right)^2 P_{\mathrm{c}}}{\sigma_{\mathrm{c}}^2}$ is the ideal SNR with perfect CSI. Substituting the channel error bound from Equation (36) yields

$$\gamma_{\mathrm{eff}} \geq \gamma_0 \left(1 - \frac{\sum_{n=1}^{N} \|\nabla h_{\mathrm{c},n}(\mathbf{u}^*)\| \varepsilon_p}{\sum_{n=1}^{N} h_{\mathrm{c},n}}\right)^2. \tag{38}$$

The BER for OOK in an AWGN channel is given by

$$\mathrm{BER} = \frac{1}{2} \mathrm{erfc}\left(\sqrt{\frac{\gamma_{\mathrm{eff}}}{2}}\right), \tag{39}$$

where $\mathrm{erfc}(\cdot)$ denotes the complementary error function. Combining Equations (38) and (39) reveals the direct dependence of BER on positioning error ε_p.

Figure 4 quantifies this relationship through simulation results, showing that a positioning error of 5 cm (typical for our ORIS-enhanced system) results in only a 0.26 dB SNR penalty, corresponding to

about 4% increase in BER at 10^{-3} target BER. This demonstrates the robustness of our integrated design, where the positioning accuracy achieved by the ORIS framework maintains communication performance within acceptable limits.

This analysis establishes the critical coupling between positioning and communication performance in VLP&C systems: positioning errors directly propagate to channel estimation errors, which subsequently degrade SNR and increase BER. The quantitative relationship derived here provides a theoretical foundation for understanding the tradeoffs in integrated system design and confirms that the positioning accuracy achieved by our ORIS-enhanced framework is sufficient to maintain reliable communication performance.

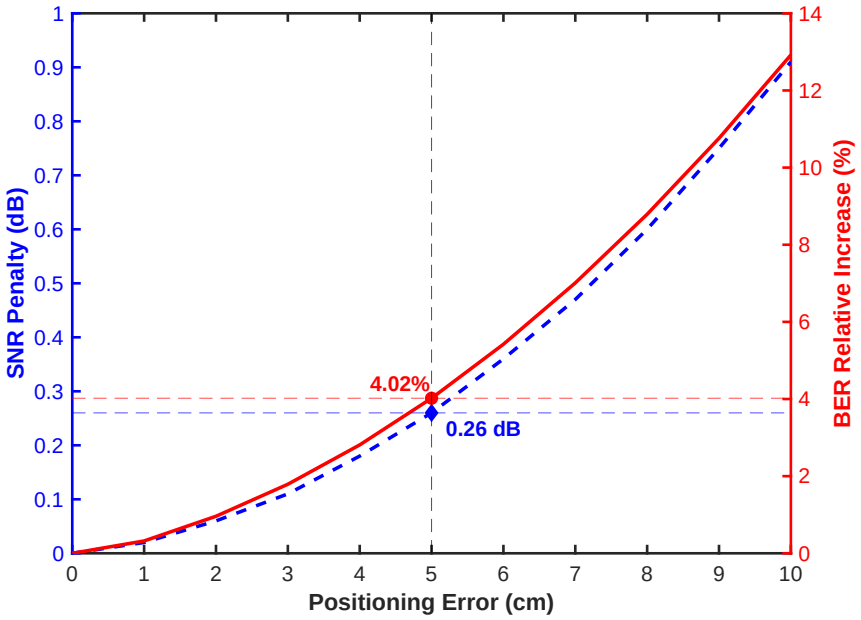

Figure 4. Relationship between positioning error on communication and positioning performance of the ORIS-assisted VLP&C system across various positioning error.

3.4. Interaction mechanism among information frames

The three information frames (positioning information frame, feedback information frame, and communication information frame) form a closed-loop system that enables the integrated VLP&C functionality. This subsection details their interaction mechanism and temporal relationship.

The three information frames operate in a sequential cycle with the following timing relationship:

(1) Positioning Phase: The LED transmits the positioning information frame, and the user's PD receives signals reflected from the ORIS. This phase lasts for T_p (typically 0.1 ms as specified in Table 1).

(2) Feedback Phase: The user's device processes the received signals to estimate its position and transmits this information back to the central controller via the infrared feedback channel. This phase lasts for T_f (typically 0.05 ms).

(3) Communication Phase: Based on the received position information, the central controller configures the ORIS and enables the communication information frame transmission. This phase lasts for T_c (typically 0.85 ms).

The total frame duration $T_{\text{frame}} = T_p + T_f + T_c$ is designed to be 1 ms, resulting in a frame rate of

1 kHz, which is sufficient for most indoor positioning and communication applications.

The interaction among the three frames follows a strict dependency chain that forms a closed-loop system.

Positioning information frame initiates the cycle by transmitting specially designed positioning signals through the LED. The user's PD receives these signals after reflection from the ORIS, enabling the estimation of the user's position with centimeter-level accuracy. As described in Section III-A, this frame employs either the 2SDRP or maximum likelihood positioning algorithm to overcome LoS blockage challenges.

Table 1. Simulation parameters and their values utilized in the simulation of the VLP&C System [45].

Parameter Category	**Value/Range**
Environment Parameters	
Room size: $(L \times W \times H)$ m^3	$5 \times 5 \times 4$ m^3
LED position: $\mathbf{s}_{\mathrm{L}}$	$[2.5, 2.5, 4]^T$ m
Central location coordinates of ORIS	$[0, 2.5, 2.5]^T$ m
LED orientation	$[0, 0, -1]^T$ m
PD height	1.5 m
User distribution	Randomly distributed
System Hardware Parameters	
Number of ORIS reflection unit: N_{R}	4×4, 8×8, 12×12
ORIS unit size: A_{r}	0.1×0.1 m^2
Reflectivity of each reflective unit: ρ	0.95
LED half-power angle: $\Theta_{1/2}$	40°, 50°, 75°
FOV of PD: Θ_{FoV}	90°
PD detection area: A_{Rx}	1 cm^2
LED transmission power: P_{total}	6 W
Optical power/electric conversion efficiency: η	813.6 μW/mA
PD responsivity: R	100 μA/mW/cm^2
Signal and Channel Parameters	
Modulation scheme	OOK
Positioning signal duration: T_{p}	0.1 ms
Speed of light: c	3×10^8 m/s
Noise variance: σ^2	10^{-14} A^2/Hz
Center frequency: f_{c}	50 MHz
Optical filter gain: $\mathscr{T}$	1
Simulation Setup Parameters	
Number of Monte Carlo trials	10,000
Positioning accuracy metric	RMSE
Communication performance metrics	BER, AMI
Algorithm Parameters	
Learning rate	0.01
Maximum iterations	50

Feedback information frame depends directly on the output of the positioning information frame. After position estimation, the user device transmits the estimated position $\hat{\mathbf{u}} = [\hat{x}, \hat{y}, \hat{z}]^T$ back to the central controller via the infrared feedback channel. As shown in Figure 3 of the original manuscript, with a 120° FoV receiver design, this feedback achieves 99.2% reliability, ensuring robust position information transfer.

Communication information frame depends on the feedback information frame, utilizing the acquired position information to optimize data transmission. Based on the received position data, the central controller calculates the optimal ORIS reflection pattern $\mathbf{W}$ and configures the ORIS accordingly. This enables the system to establish the best possible NLoS communication link for the user's current location.

The communication frame completes the cycle by providing updated channel state information that influences the next positioning frame. This creates a continuous closed-loop system.

4. Performance analysis

4.1. Performance analysis of the ORIS-assisted positioning subsystem

The positioning accuracy of the ORIS-assisted VLP&C system is evaluated using the CRLB, which provides a fundamental limit on the variance of any unbiased position estimator [7]. Unlike previous works that assume Gaussian-distributed distance estimates with known variance [46], we derive the CRLB directly from the signal expressions to obtain a more realistic performance bound.

Let $\mathbf{y} = [y_1, y_2, \ldots, y_N]^T$ denote the received signal vector at the PD, where y_n represents the signal received via the nth ORIS reflection unit. The conditional probability density function (PDF) of $\mathbf{y}$ given the user position $\mathbf{u}$ can be expressed as

$$p(\mathbf{y}|\mathbf{u}) = \prod_{n=1}^{N} \frac{1}{\sqrt{2\pi\sigma^2}} \exp\left(-\frac{(y_n - \hat{h}_{\mathrm{c},n}(\mathbf{u})s)^2}{2\sigma_{\mathrm{c}}^2} \right), \tag{40}$$

where s is the transmitted signal, σ_{c}^2 is the noise variance, and $\hat{h}_{\mathrm{c},n}(\mathbf{u})$ is the estimated channel gain for the nth reflection path, given by Equation (31).

The log-likelihood function is then derived by

$$\Lambda(\mathbf{u}) = \ln p(\mathbf{y}|\mathbf{u}) = -\frac{N}{2}\ln(2\pi\sigma_{\mathrm{c}}^2) - \frac{1}{2\sigma_{\mathrm{c}}^2}\sum_{n=1}^{N}(y_n - \hat{h}_{\mathrm{c},n}(\mathbf{u})s)^2. \tag{41}$$

The Fisher information matrix (FIM) $\mathbf{I}(\mathbf{u})$ is computed as the negative expectation of the second derivative of the log-likelihood function

$$[\mathbf{I}(\mathbf{u})]_{i,j} = -\mathbb{E}\left[\frac{\partial^2 \Lambda(\mathbf{u})}{\partial u_i \partial u_j} \right], \tag{42}$$

where the variables u_i and u_j for $i, j = 1, 2, 3$ correspond to spatial coordinates $u_1 = x$, $u_2 = y$, and $u_3 = z$, respectively.

The partial derivatives of the distances with respect to the positional coordinates are given by

$$\frac{\partial d_{\mathrm{SR}_n}}{\partial u_i} = 0, \tag{43}$$

since d_{SR_n} is independent of user position, and

$$\frac{\partial \hat{d}_{\mathrm{R}_n\mathrm{D}}}{\partial u_i} = \frac{u_i - R_i^n}{\hat{d}_{\mathrm{R}_n\mathrm{D}}}, \tag{44}$$

where the variables R_i^n for $i = 1,2,3$ correspond to spatial coordinates of the nth ORIS reflective unit position and $R_1^n = R_x^n$, $R_2^n = R_y^n$, and $R_3^n = R_z^n$, respectively.

The angle derivatives are given by

$$\frac{\partial \phi_{\mathrm{LED}}^{(n)}}{\partial u_i} = \frac{-(R_i^n - \mathbf{s}_{\mathrm{L},i})}{d_{\mathrm{SR}_n}^2 \sin(\phi_{\mathrm{LED}}^{(n)})} \cdot \frac{\partial d_{\mathrm{SR}_n}}{\partial u_i} = 0, \tag{45}$$

$$\frac{\partial \hat{\alpha}_{\mathrm{PD}}^{(n)}}{\partial u_i} = \frac{-(u_i - R_i^n)}{\hat{d}_{\mathrm{R}_n\mathrm{D}}^2 \sin(\hat{\alpha}_{\mathrm{PD}}^{(n)})}, \tag{46}$$

$$\frac{\partial \theta_1^{(n)}}{\partial u_i} = \frac{-(\mathbf{s}_{\mathrm{L},i} - R_i^n) \cdot \mathbf{n}_{\mathrm{ORIS},i}}{d_{\mathrm{SR}_n}^2 \sin(\theta_1^{(n)})} \cdot \frac{\partial d_{\mathrm{SR}_n}}{\partial u_i} = 0, \tag{47}$$

$$\frac{\partial \hat{\theta}_2^{(n)}}{\partial u_i} = \frac{-(u_i - R_i^n) \cdot \mathbf{n}_{\mathrm{ORIS},i}}{\hat{d}_{\mathrm{R}_n\mathrm{D}}^2 \sin(\hat{\theta}_2^{(n)})}, \tag{48}$$

where $\mathbf{n}_{\mathrm{ORIS}}$ is the normal vector of the ORIS plane, and $\mathbf{n}_{\mathrm{ORIS},i}$ ($i = 1,2,3$) is the ith entry of $\mathbf{n}_{\mathrm{ORIS}}$. $\mathbf{s}_{\mathrm{L},i}$ for $i = 1,2,3$ correspond to spatial coordinates of the LED position and $\mathbf{s}_{\mathrm{L},1} = x_{\mathrm{L}}$, $\mathbf{s}_{\mathrm{L},2} = y_{\mathrm{L}}$, and $\mathbf{s}_{\mathrm{L},3} = z_{\mathrm{L}}$, respectively. Additionally, $\frac{\partial d_{\mathrm{SR}_n}}{\partial u_i}$ and $\frac{\partial \hat{d}_{\mathrm{R}_n\mathrm{D}}}{\partial u_i}$ represent the partial derivatives of respective distances with respect to these position coordinates.

After detailed derivation, the FIM elements are given by

$$[\mathbf{I}(\mathbf{u})]_{i,j} = \frac{s^2}{\sigma_{\mathrm{c}}^2} \sum_{n=1}^{N} \frac{\partial \hat{h}_{\mathrm{c},n}(\mathbf{u})}{\partial u_i} \frac{\partial \hat{h}_{\mathrm{c},n}(\mathbf{u})}{\partial u_j}. \tag{49}$$

The partial derivatives of $\hat{h}_{\mathrm{c},n}(\mathbf{u})$ with respect to position coordinates can be computed as follows. For the x-coordinate

$$\begin{aligned}
\frac{\partial \hat{h}_{\mathrm{c},n}(\mathbf{u})}{\partial x} &= \hat{h}_{\mathrm{c},n}(\mathbf{u}) \Bigg[-\frac{2(x - R_x^n)}{d_{\mathrm{SR}_n}^2 \hat{d}_{\mathrm{R}_n\mathrm{D}}} \cdot \frac{\partial \hat{d}_{\mathrm{R}_n\mathrm{D}}}{\partial x} \\
&\quad - m \tan(\phi_{\mathrm{LED}}^{(n)}) \frac{\partial \phi_{\mathrm{LED}}^{(n)}}{\partial x} - \tan(\hat{\alpha}_{\mathrm{PD}}^{(n)}) \frac{\partial \hat{\alpha}_{\mathrm{PD}}^{(n)}}{\partial x} \\
&\quad - \tan(\theta_1^{(n)}) \frac{\partial \theta_1^{(n)}}{\partial x} - \tan(\hat{\theta}_2^{(n)}) \frac{\partial \hat{\theta}_2^{(n)}}{\partial x} \Bigg] \\
&= \hat{h}_{\mathrm{c},n}(\mathbf{u}) \Bigg[-\frac{2(x - R_x^n)}{\hat{d}_{\mathrm{R}_n\mathrm{D}}^2} + \frac{(x - R_x^n)}{\hat{d}_{\mathrm{R}_n\mathrm{D}}^2 \cos(\hat{\alpha}_{\mathrm{PD}}^{(n)})} \\
&\quad + \frac{(x - R_x^n) \cdot \mathbf{n}_{\mathrm{ORIS},x}}{\hat{d}_{\mathrm{R}_n\mathrm{D}}^2 \cos(\hat{\theta}_2^{(n)})} \Bigg]
\end{aligned} \tag{50}$$

Similarly, for the y- and z-coordinates, the derivatives are

$$\frac{\partial \hat{h}_{c,n}(\mathbf{u})}{\partial y} = \hat{h}_{c,n}(\mathbf{u}) \left[-\frac{2(y - R_y^n)}{\hat{d}^2_{R_nD}} + \frac{(y - R_y^n)}{\hat{d}^2_{R_nD} \cos(\hat{\alpha}^{(n)}_{PD})} + \frac{(y - R_y^n) \cdot \mathbf{n}_{ORIS,y}}{\hat{d}^2_{R_nD} \cos(\hat{\theta}^{(n)}_2)} \right]. \tag{51}$$

and

$$\frac{\partial \hat{h}_{c,n}(\mathbf{u})}{\partial z} = \hat{h}_{c,n}(\mathbf{u}) \left[-\frac{2(z - R_z^n)}{\hat{d}^2_{R_nD}} + \frac{(z - R_z^n)}{\hat{d}^2_{R_nD} \cos(\hat{\alpha}^{(n)}_{PD})} + \frac{(z - R_z^n) \cdot \mathbf{n}_{ORIS,z}}{\hat{d}^2_{R_nD} \cos(\hat{\theta}^{(n)}_2)} \right]. \tag{52}$$

respectively.

Then, the CRLB for the position estimate is given by the diagonal elements of the inverse FIM

$$\text{var}(\hat{u}_i) \geq [\mathbf{I}(\mathbf{u})^{-1}]_{i,i}. \tag{53}$$

Finally, the total positioning error bound is derived as

$$\varepsilon_{CRLB} = \sqrt{[\mathbf{I}(\mathbf{u})^{-1}]_{1,1} + [\mathbf{I}(\mathbf{u})^{-1}]_{2,2} + [\mathbf{I}(\mathbf{u})^{-1}]_{3,3}}. \tag{54}$$

4.2. Performance analysis of the ORIS-assisted communication subsystem

The AMI between the transmitted and received signals characterizes the communication capacity of the ORIS-assisted VLP&C system. For an OOK-modulated system, the AMI is given by

$$\mathbb{I}(X;Y) = \mathbb{H}(Y) - \mathbb{H}(Y|X), \tag{55}$$

where $\mathbb{H}(Y)$ is the entropy of the received signal and $\mathbb{H}(Y|X)$ is the conditional entropy.

Given the channel model in Equation (34), the conditional PDF of the received signal given the transmitted symbol can be expressed as

$$p(y|0) = \frac{1}{\sqrt{2\pi\sigma_c^2}} \exp\left(-\frac{y^2}{2\sigma_c^2} \right), \tag{56}$$

$$p(y|1) = \frac{1}{\sqrt{2\pi\sigma_c^2}} \exp\left(-\frac{(y - h_{tot}s)^2}{2\sigma_c^2} \right), \tag{57}$$

where $h_{tot} = \sum_{n=1}^{N} h_{c,n}(\mathbf{u})$ is the total channel gain.

The AMI can then be computed as

$$\mathbb{I}(X;Y) = \frac{1}{2} \int_{-\infty}^{\infty} \left[p(y|0) \log_2 \frac{2p(y|0)}{p(y|0) + p(y|1)} + p(y|1) \log_2 \frac{2p(y|1)}{p(y|0) + p(y|1)} \right] dy. \tag{58}$$

While Equation (58) does not have a closed-form solution, we can derive a tight LB using the entropy power inequality

$$\begin{aligned} \mathbb{I}(X;Y) &= \mathbb{H}(Y) - \mathbb{H}(Y|X) \\ &\geq \frac{1}{2} \log_2 \left(2^{2h(Y|X)} + \frac{(h_{tot}s)^2}{2\pi e} \right) - \mathbb{H}(Y|X) \\ &= \frac{1}{2} \log_2 \left(1 + \frac{(h_{tot}s)^2}{2\pi e \sigma_c^2} \right) \\ &\approx \frac{1}{2} \log_2 \left(1 + \frac{(h_{tot}s)^2}{4\sigma_c^2} \right) \end{aligned} \tag{59}$$

This lower bound becomes increasingly tight as the SNR increases, as shown in our simulations.

5. Simulations results

To assess the performance provided by the ORIS-assisted VLP&C system in an indoor LoS blockage setting, comprehensive simulation experiments are conducted in this section utilizing the Monte Carlo simulation method tailored for indoor environments. The room's dimensions are defined as $(5 \times 5 \times 4)$ m^3, with the LED transmitter installed on the ceiling of the indoor service area. The normal vector of the ORIS reflective unit is oriented perpendicularly to the wall, while the PD is installed at the user receiver in a vertical orientation directed upwards. Unless stated otherwise, the primary system parameters utilized in the simulation are outlined in Table 1. Considering the common occurrence of blockages in indoor settings, our simulation is predominantly centered on the ORIS-assisted single-reflection NLoS link, predicated on the assumption that the LoS link between the LED and the PD is blocked.

5.1. Simulation analysis of positioning results

In this section, the simulation results of the positioning performance of the ORIS-assisted VLP&C system are presented to verify the effectiveness of the presented positioning algorithms and the accuracy of the CRLB theoretical analysis results. Among them, the transmission signal $s_{\mathrm{p}}(t)$ in Equation (6) is modeled as [47]

$$s_{\mathrm{p}}(t) = P_{\mathrm{p}}(1-\cos(2\pi t/T_{\mathrm{p}}))(1+\cos(2\pi f_{\mathrm{c}} t)), t \in [0, T_{\mathrm{p}}], \tag{60}$$

where f_{c} denotes the center frequency, P_{p} signifies the average transmitted optical power, which refers to the output power of the light source, and T_{p} represents the duration of the transmitted positioning signal.

Figure 5 illustrates the relationship between positioning error and the SNR for two methodologies derived from the three-dimensional 2SDRP algorithm and the maximum likelihood positioning algorithm, evaluated across four distinct quantities of ORIS reflective units, with the location coordinates of user 1 specified as $(1.0, 2.5, 1.5)$ m. Initially, it is evident from Figure 5 that as SNR increases, the positioning errors for both methodologies exhibit a pattern of rapid decline followed by stabilization. This trend can be attributed to the diminishing impact of noise on positioning performance as SNR increases, leading to more accurate distance estimations between the ORIS reflective unit and the PD, thereby enhancing overall positioning accuracy. Furthermore, Figure 5 indicates that the maximum likelihood positioning method outperforms the 2SDRP algorithm at lower SNR levels. However, at higher SNR levels, the performance of both methods converges, demonstrating consistent positioning estimation capabilities. This disparity in performance can be explained by the fact that the maximum likelihood positioning approach employs a more comprehensive distance condition compared to the 2SDRP algorithm, thereby more effectively mitigating the effects of distance errors on positioning accuracy.

It is important to note that while the ORIS-assisted three-dimensional 2SDRP algorithm exhibits marginally inferior performance compared to the maximum likelihood positioning algorithm, while the 2SDRP algorithm demonstrates greater adaptability to varying conditions. Specifically, the positioning function can be executed using either four reference points or a greater number of reference points with arbitrary configurations. In contrast, the maximum likelihood method is constrained by its requirement to operate under a fixed configuration of reference points, which is dictated by the conditional limitations inherent in its derivation process.

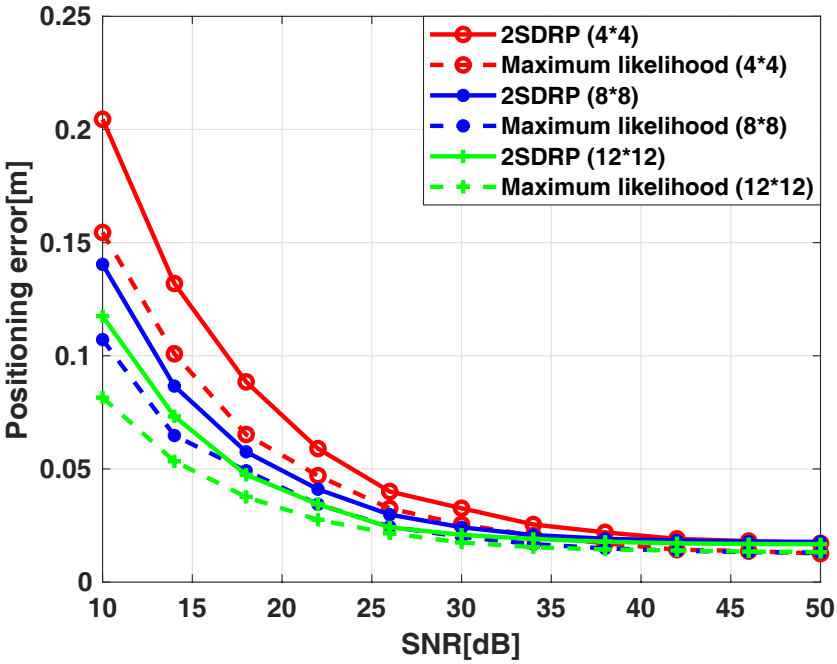

Figure 5. Relationship between positioning error and SNR with different quantities of ORIS reflective units for user 1.

Furthermore, as illustrated in Figure 5, it is evident that when the ORIS satisfies the communication requirements, its sizes significantly influence the system's positioning performance. Specifically, an increase in the size of ORIS correlates with enhanced positioning accuracy for the two methodologies discussed in this paper. This improvement can be attributed to the greater number of reflective units within ORIS, which facilitates the activation of a larger array of scattered reflective units for positioning, thereby diminishing the correlation among different channels. However, it is imperative to acknowledge that excessively enlarging the size of ORIS in pursuit of improved positioning performance may not be advisable. Consideration must be given to the associated hardware costs and complexity to avoid excessive spatial occupation, which could hinder the feasibility of practical applications.

To further assess the validity of the aforementioned conclusions, user 2 and user 3 are selected for evaluation under the same simulation parameters as depicted in Figure 5. The respective position coordinates for user 2 and user 3 are $(1.5, 2.0, 1.5)$ m and $(2.0, 1.5, 1.5)$ m, respectively. Analysis of Figure 6 and Figure 7 indicates that an increase in either the SNR or the number of ORIS reflective units can enhance positioning performance, with the underlying reasons aligning closely with the findings presented in Figure 5. Furthermore, a comparative analysis of Figures 5, 6 and 7 reveals a gradual increase in positioning error as the distance between the PD and the ORIS reflective unit increases. This trend can be attributed to the diminishing radiant light power received by the user's PD as they move further from the ORIS reflective unit, which leads to a reduced SNR and a corresponding decline in positioning accuracy. Additionally, it is noteworthy that when the SNR reaches a certain threshold, the noise level becomes sufficiently low, resulting in negligible improvements in performance despite an increase in the number of ORIS reflective units, as illustrated in Figures 5, 6 and 7.

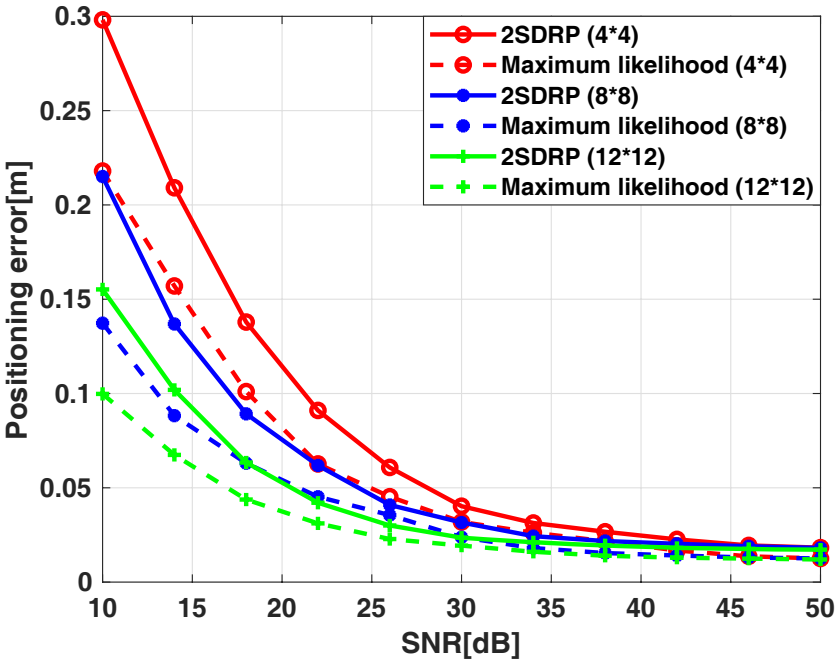

Figure 6. Relationship between positioning error and SNR with different quantities of ORIS reflective units for user 2.

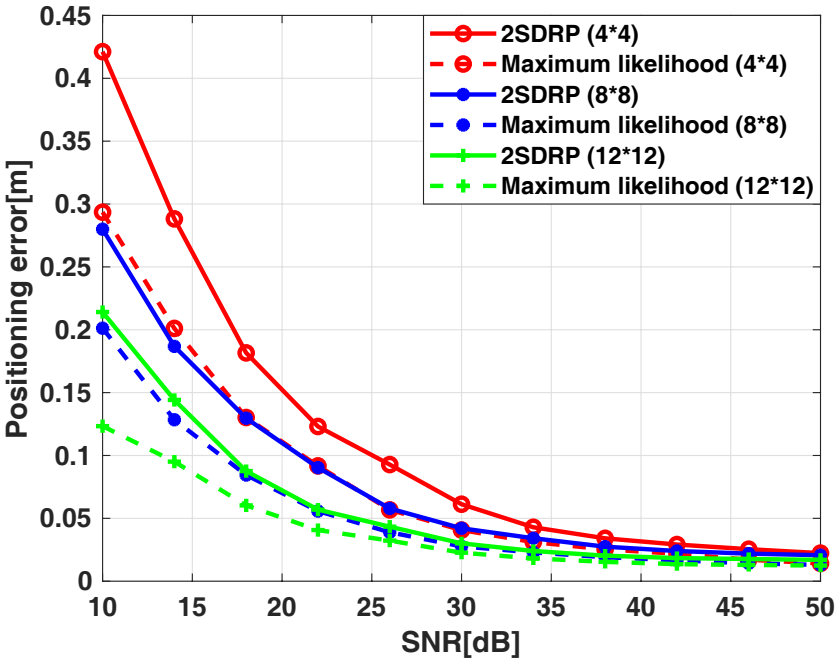

Figure 7. Relationship between positioning error and SNR with different quantities of ORIS reflective units for user 3.

Subsequently, the performance of the proposed ORIS-assisted positioning method is elucidated through a simulation analysis of the CRLB. Concurrently, the accuracy of the derived theoretical expression for the CRLB is validated in accordance with the mathematical model pertaining to the VLP&C positioning problem. To facilitate this analysis, the height of the PD receiver is maintained at 1.5 m, and the configuration of ORIS reflective units is established at 8×8. Figure 8 illustrates the relationship between the positioning error of the maximum likelihood estimation method and the CRLB

across various user position coordinates. Given that the performance of the 2SDRP algorithm has been demonstrated to be marginally inferior to that of the maximum likelihood positioning method, the latter, which exhibits reduced error, is selected for comparative purposes to enhance the clarity of the simulation results. As depicted in Figure 8, an increase in the SNR facilitates the convergence of the positioning algorithm towards the established CRLB across different user locations.

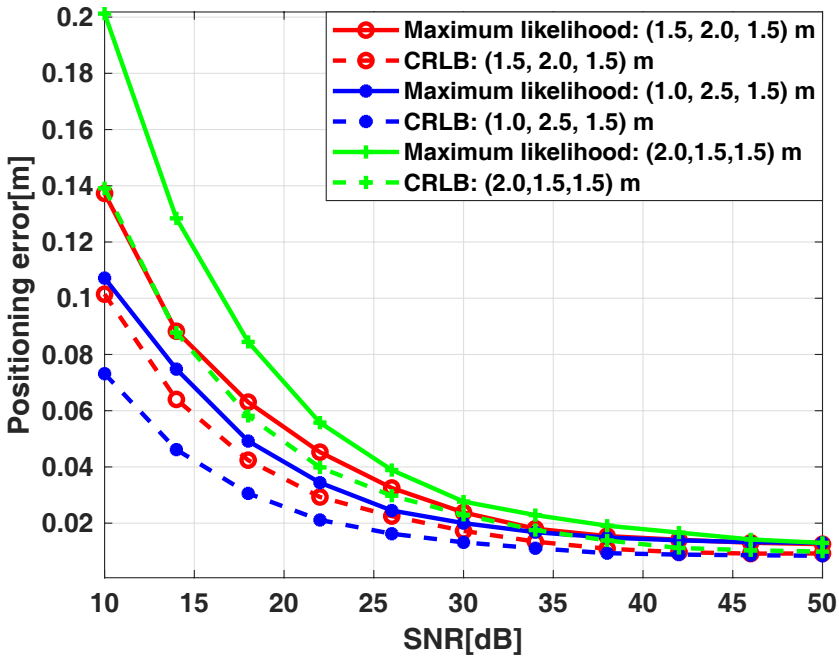

Figure 8. Relationship between positioning error and positioning CRLB of the ORIS-assisted VLP&C system across various user locations.

To further evaluate the performance of the proposed positioning algorithm across the entire service area and to gain insights into the impact of the ORIS on positioning accuracy in scenarios where the LoS link is blocked, this simulation examines the positioning error of the considered system as the user traverses a designated horizontal plane within a service room, during which the maximum likelihood positioning algorithm is implemented. Specifically, a total of 1,089 user location points are analyzed on this plane, with a spacing of 0.15 m between adjacent points, a height of the PD set at 1.5 m, and a SNR of 30 dB. The variations in positioning error relative to the PD's location in both three-dimensional and two-dimensional contexts are illustrated in Figure 9, revealing an average positioning error of approximately 0.07 m. As depicted in Figure 9, it is evident that when the PD is positioned at a larger distance from the wall equipped with ORIS, the positioning error increases, suggesting a strong correlation between the positioning performance of the ORIS-assisted NLoS link and the distance separating the PD receiver from the ORIS reflective units. Conversely, when the PD is situated closer to the center of the ORIS, the contribution of ORIS to positioning accuracy becomes pronounced, leading to a marked enhancement in positioning performance. Furthermore, Figure 9 indicates that the positioning error at the corners of the wall where ORIS is installed is significantly greater than at other locations within the service area. This phenomenon can be attributed to the presence of channel correlation and reflection blind area associated with ORIS, which results in a relatively weak reflected signal for users situated in these regions, thereby exacerbating the positioning error. However, this can be effectively improved by equipping two or more ORIS on different walls in the room.

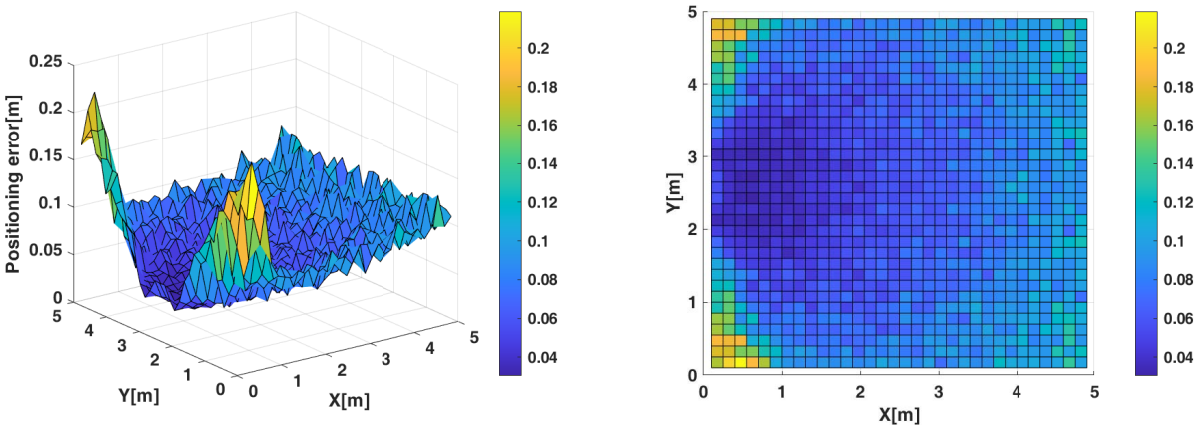

(a) (b)

Figure 9. User positioning error distribution at the same height z, where $z = 1.5$ m. **(a)** Three-dimensional positioning error distribution diagram of the ORIS-assisted VLP&C system; **(b)** Two-dimensional positioning error distribution diagram of the ORIS-assisted VLP&C system.

In the same experimental conditions, Figure 10 and Figure 11 illustrate the distribution of positioning errors for users located throughout the room, with the PD height set at 1 m and 0.5 m, respectively. Consistent with the simulation findings at a height of 1.5 m, the mean positioning errors recorded are 0.10 m and 0.14 m, respectively. Furthermore, a comparative analysis of Figures 9, 10, and 11 reveals that PD receivers positioned at identical locations exhibit varying positioning errors when installed at different heights. Notably, an increase in height correlates with improved positioning performance. However, it is crucial to recognize that excessively elevating the position height to enhance positioning accuracy may lead to the reflected signal exiting the PD's FoV, resulting in a channel gain of zero and rendering the positioning function ineffective.

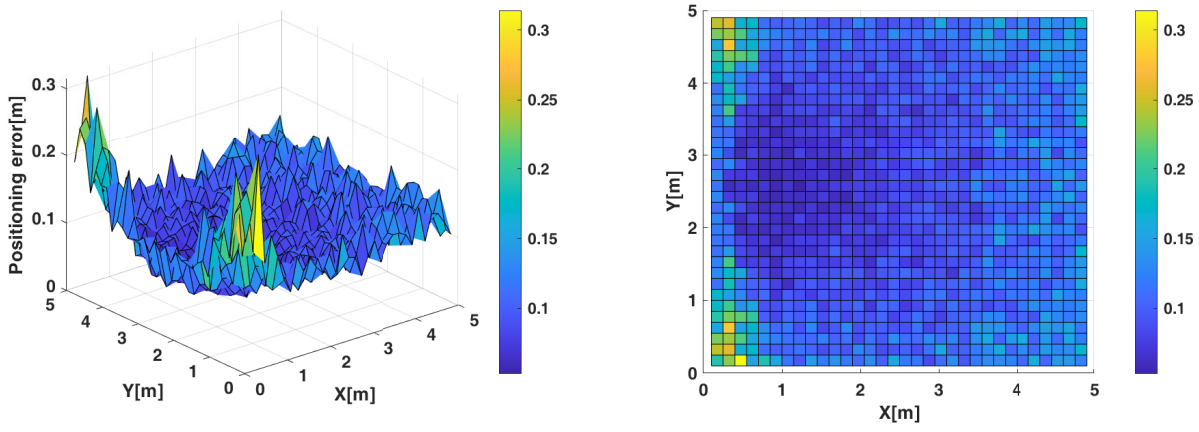

(a) (b)

Figure 10. User positioning error distribution at the same height z, where $z = 1.0$ m. **(a)** Three-dimensional positioning error distribution diagram of the ORIS-assisted VLP&C system; **(b)** Two-dimensional positioning error distribution diagram of the ORIS-assisted VLP&C system.

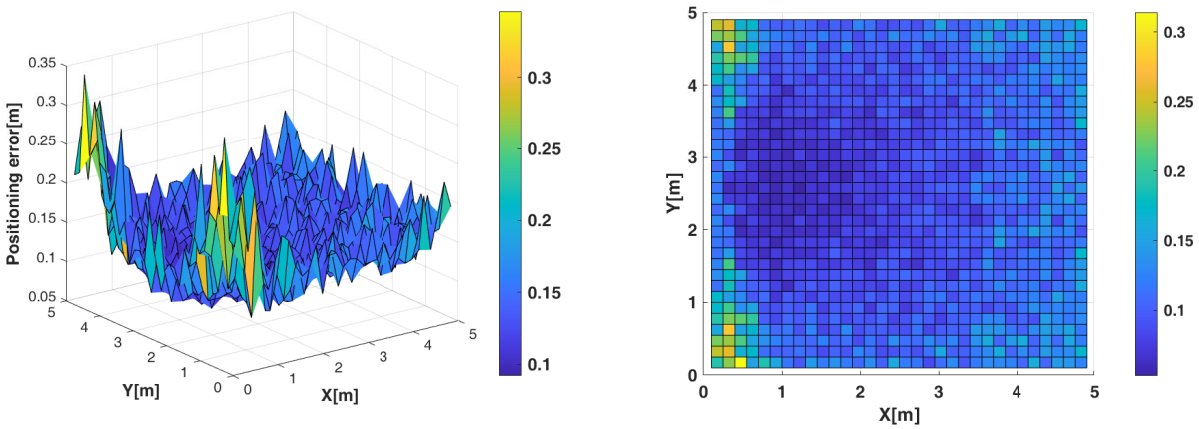

(a) (b)

Figure 11. User positioning error distribution at the same height z, where $z = 0.5$ m. **(a)** Three-dimensional positioning error distribution diagram of the ORIS-assisted VLP&C system; **(b)** Two-dimensional positioning error distribution diagram of the ORIS-assisted VLP&C system.

Figure 12 illustrates the relationship between the cumulative distribution function (CDF) curve of positioning error and the height of the user's PD receiver, based on the previously analyzed three-dimensional error results in Figures 9, 10 and 11. The positioning errors at test points across the entire plane are measured at heights of 0.5 m, 1.0 m, and 1.5 m, yielding results where 90 % of the positioning errors are recorded as 0.223 m, 0.168 m, and 0.127 m, respectively. Given that the spatial distribution of LED luminous intensity remains constant, the signal strength received by the PD will vary in accordance with the user's positional changes. As depicted in Figure 12, it is evident that a smaller height differential between the user and the ORIS correlates with a reduced distance and consequently enhances positioning accuracy.

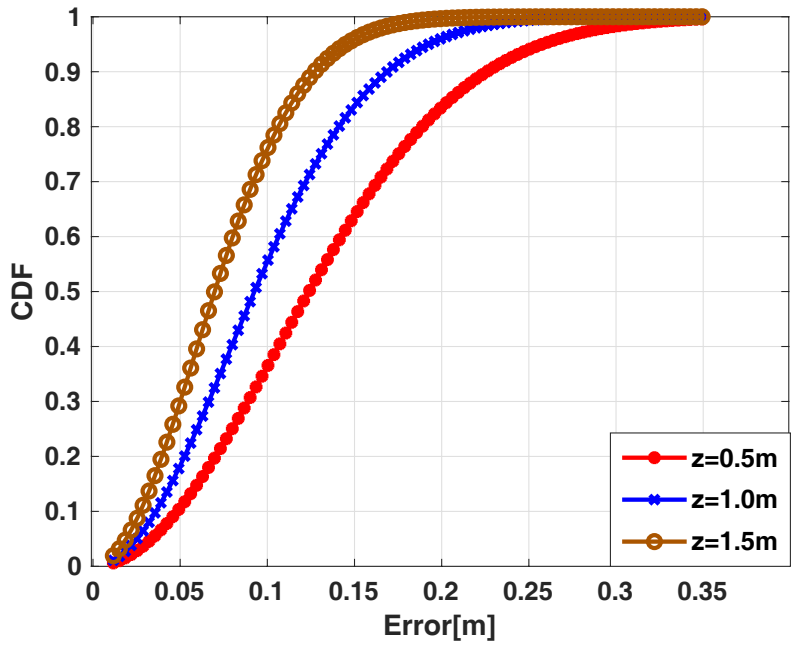

Figure 12. Comparative analysis of the CDF curves of positioning errors at various user heights.

5.2. Communication performance simulation analysis

This part aims to assess the communication performance of the ORIS-assisted VLP&C system through simulation analysis, following an evaluation of system positioning performance. It will examine the impact of varying the number of ORIS reflective units and the half-power angle of the LED on the communication system's efficacy. Additionally, a comparative analysis of system's BER performance across different link environments will be conducted, alongside an evaluation of the system's AMI and its LB.

To assess the impact of varying quantities of ORIS reflective units on system communication performance, simulations are conducted to evaluate the BER performance of the system utilizing 16 (4×4), 64 (8×8), and 144 (12×12) ORIS reflective units, with user position coordinates set at $(1.0, 2.5, 1.5)$ m. Figure 13 illustrates the BER performance of the proposed ORIS-assisted VLC system across different configurations of ORIS reflective units. The results presented in Figure 13 indicate a notable enhancement in BER performance corresponding to an increase in the number of ORIS reflective units. This improvement can be attributed to the augmented signal power received by the PD as the number of ORIS reflective units increases, thereby significantly enhancing the system's BER performance. In practical applications, the optimal number of ORIS reflective units should be determined based on specific application requirements.

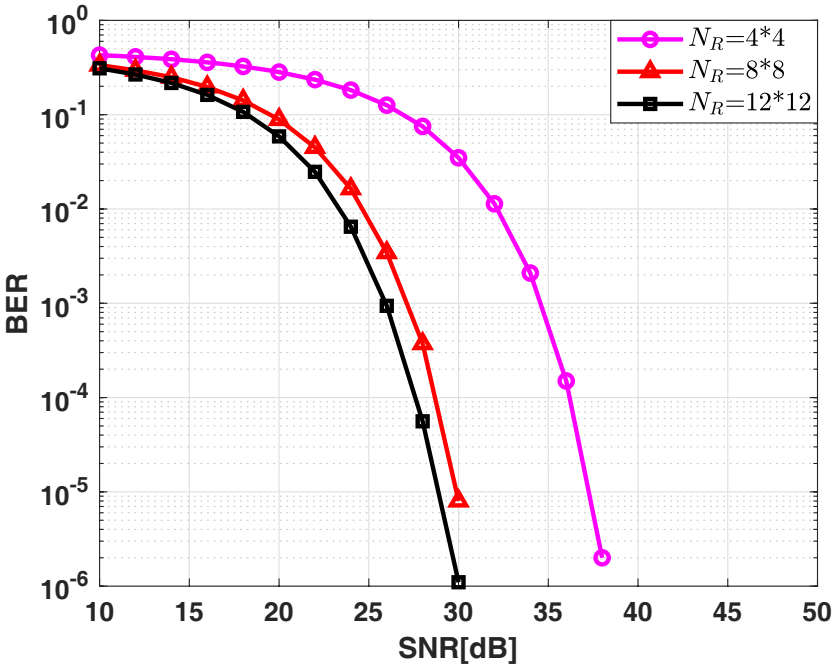

Figure 13. Comparisons of BER performance with different number of ORIS reflective units.

To further investigate the impact of system parameters on the performance of the communication system, Figure 14 illustrates the effect of varying LED half-power angles on the BER performance. For the purposes of this analysis, the configuration is maintained at 8×8 ORIS reflective units. The half-power angles of the system are established at predetermined values of 40°, 50° and 75°. Concurrently, the locations and orientations of the normal vectors for both the LED transmitter and the PD receiver are maintained as constant. As depicted in Figure 14, a larger coverage range associated with the half-power

angle correlates with improved BER performance. However, when $\Phi_{1/2} = 40°$, certain signals may remain undetected due to the half-power angle's influence, which can prevent the signal emitted by the LED from directly reaching the corresponding ORIS reflective unit. Consequently, the selection of the half-power angle is critical, as it directly influences the signal radiation range of the ORIS-assisted VLP&C system and the power of the received signal at the receiver, thereby affecting the overall BER performance of the system.

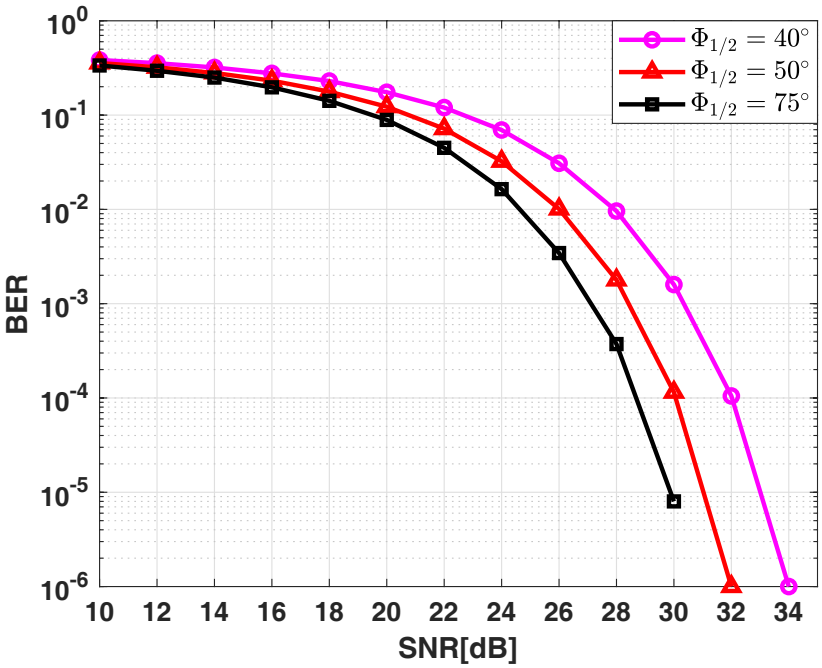

Figure 14. BER performance comparisons of the ORIS-assisted VLP&C system with different half-power angle $\Phi_{1/2}$ of LED, where $\Phi_{1/2} = 40°, 50°$, and $75°$.

Figure 15 presents a comparative analysis of the BER performance of VLP&C systems across three distinct communication link environments: an ORIS-assisted NLoS link, a LoS link, and a diffuse link. For the purposes of this comparison, it is assumed that a LoS link is available to the user. The simulation results indicate that the BER performance of the system is optimal in the non-blocked LoS environment. In contrast, the performance of BER experiences a substantial decline when dependent exclusively on a diffuse reflection link in the event of blockage. This decline is primarily attributed to the optical path loss associated with diffuse reflection, which is influenced by various physical factors, including room dimensions and the reflectivity of the ceiling and walls. In scenarios involving blockage of the LoS link, the proposed ORIS auxiliary scheme demonstrates a substantial enhancement in the system's BER performance. Specifically, at a BER of 10^{-5}, the ORIS-assisted NLoS reflection link achieves an improvement of 7 dB in BER performance than the diffuse reflection link.

Finally, Figure 16 illustrates the outcomes of a simulation analysis regarding the variations in communication AMI and its LB of an ORIS-assisted indoor VLP&C system as a function of the number of ORIS reflective units. The data presented in the figure indicates that both the AMI of the system and its LB initially increase with the enhancement of the SNR, ultimately converging towards a constant value of 1 bits/symbol at elevated SNR levels. Furthermore, it is evident that an increase in the number of ORIS reflective units results in a reduction of the SNR required for the communication system to attain its

maximum AMI. This phenomenon can be attributed to the corresponding increase in the receiving power at the PD as the number of ORIS reflective units rises, thereby diminishing the system's dependency on transmitting power. Additionally, Figure 16 reveals that the disparity between the parameters $\mathbb{I}(h_c^r;Y)$ and $\mathbb{I}_L(h_c^r;Y)$ in both high and low SNR regions is approximately $(\log_2 e - 1)/2$.

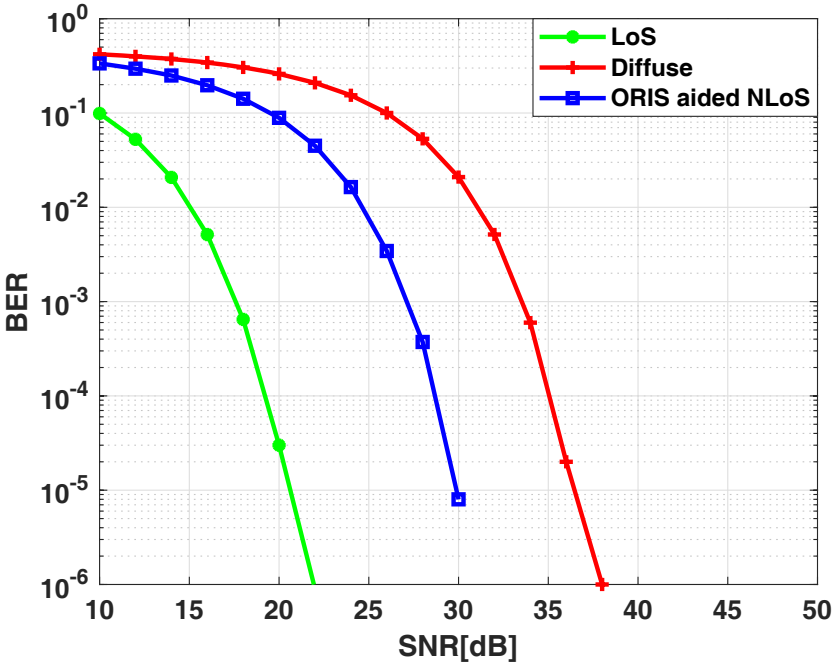

Figure 15. BER performance comparison versus SNR under different propagation environments.

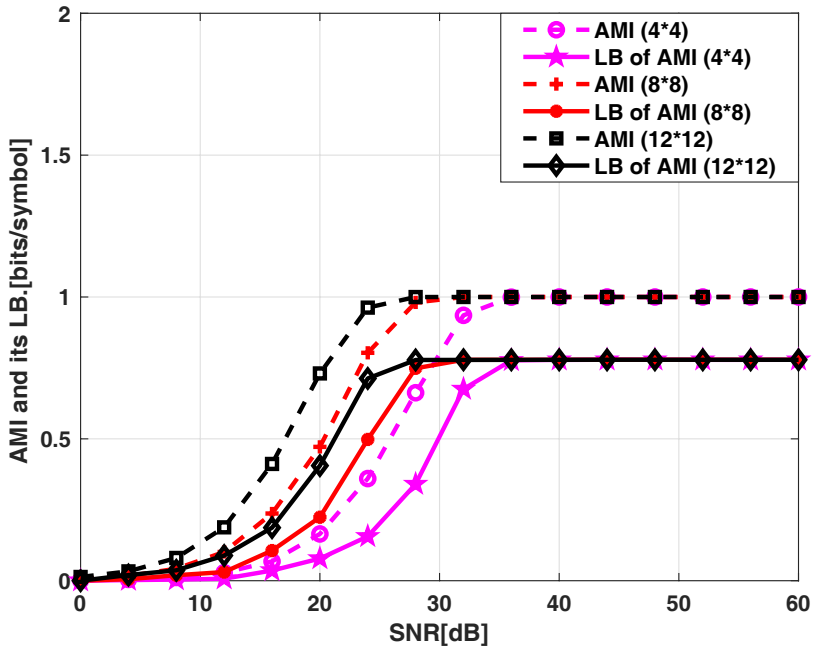

Figure 16. The relationship between the communication AMI and its LB versus SNR at different number of ORIS reflective units.

6. Conclusions

This study primarily focuses on the design of an integrated VLP&C system by introducing an ORIS to establish a novel NLoS visible light reflection transmission link in scenarios where the LoS link was blocked within complex indoor environments. The proposed approach aimed to facilitate efficient communication and high-precision positioning within the system. A channel model was developed based on the controllable characteristics of the visible light reflection channel, which provided the foundation for constructing the system model as well as for the design and implementation of communication functionalities. The information frame structure was carefully designed to include positioning information frames, feedback information frames, and communication information frames, thereby supporting the distinct functions of positioning and communication. Initially, the positioning information frame employed a three-dimensional 2SDRP positioning method combined with a maximum likelihood estimation technique to achieve high-precision positioning for users experiencing LoS link blockage. The CRLB for positioning performance was analyzed and presented, followed by an evaluation of the system's positioning capabilities. Subsequently, the communication function, predicated based on ORIS, was realized through feedback derived from user position estimation results. A theoretical evaluation of the system's communication performance was conducted by deriving the AMI and its closed-form LB. Finally, extensive simulation results demonstrated that the ORIS effectively mitigates the challenges associated with LoS link blockage in VLP&C systems operating within complex indoor environments, while concurrently preserving the overall performance integrity of the VLP&C system.

Additionally, our system can complement other positioning technologies in 6G networks (such as mmWave positioning and UWB positioning) to construct hybrid positioning systems with multiple technologies, providing seamless indoor-outdoor positioning experiences. Future work will explore these integrations to develop a truly unified 6G positioning and communication architecture. Furthermore, our current analysis focuses on a single ORIS deployment. However, in larger indoor spaces, multiple ORIS units deployed on different walls could provide complementary coverage and enhanced reliability. Future research should investigate optimal placement strategies, cooperative control mechanisms, and potential interference management between multiple ORIS units.

Acknowledgments

This research was partially funded by the National Natural Science Foundation of Henan Province under Grants 252102211122 and 242102210210, the National Natural Science Foundation of China under Grant 62571182, and Opening Project of Henan Province Engineering Technology Research Center for Photoelectric Detection and Sensing Integration, Henan Polytechnic University KFZ202501.

Authors' contribution

Fasong Wang: conceptualization, methodology, investigation, software, validation, writing—original and draft preparation, supervision and funding acquisition. Wen Jiang: software, writing—original draft preparation, methodology and writing—reviewing. Rui Li: methodology, writing—reviewing and editing.

Xingwang Li: methodology, editing, supervision and funding acquisition. Arumugam Nallanathan: validation, writing—reviewing and supervision. All authors have read and agreed to the published version of the manuscript.

Conflicts of interests

Xingwang Li and Arumugam Nallanathan, Executive Editor-in-Chief and Editor-in-Chief of Advanced Information and Communication, have not peer reviewed or made any editorial decisions for this paper.

References

[1] Li X, Zheng Y, Khan WU, Zeng M, Li D, *et al.* Physical layer security of cognitive ambient backscatter communications for green internet-of-things. *IEEE Trans. Green Commun. Networking* 2021, 5(3):1066–1076.

[2] Yang H, Zhong W, Chen C, Alphones A. Integration of visible light communication and positioning within 5G networks for Internet of Things. *IEEE Network* 2020, 34(5):134–140.

[3] Zhuang Y, Hua L, Qi L, Yang J, Cao P, *et al.* A survey of positioning systems using visible LED lights. *IEEE Commun. Surv. Tutorials* 2018, 20(3):1963–1988.

[4] Bastiaens S, Alijani M, Joseph W, Plets D. Visible light positioning as a next-generation indoor positioning technology: a tutorial. *IEEE Commun. Surv. Tutorials* 2024, 26(4):2867–2913.

[5] Memedi A, Dressler F. Vehicular visible light communications: a survey. *IEEE Commun. Surv. Tutorials* 2021, 23(1):161–181.

[6] Shi C, Zhang K, Zhu B, Zhang Z. A simultaneous visible light positioning and LED database construction scheme. *IEEE J. Sel. Areas Commun.* 2024, 42(9):2520–2534.

[7] Liang Z, Lu H, Kong H, Zhou J, Liu X, *et al.* Rate optimization based on successive convex approximation algorithm in the self-powered visible light communication and positioning system. *IEEE Trans. Wireless Commun.* 2024, 23(11):16559–16574.

[8] Shi S, Gui G, Lin Y, Yuen C, Dobre OA, *et al.* Joint beamformer design and power allocation method for hybrid RF-VLCP system. *IEEE Internet Things J.* 2024, 11(5):7878–7892.

[9] Zhu Z, Yang Y, Chen M, Guo C, Cheng J, *et al.* A Survey on indoor visible light positioning systems: fundamentals, applications, and challenges. *IEEE Commun. Surv. Tutorials* 2024, 27(3):1656–1686.

[10] Italiano L, Tedeschini BC, Brambilla M, Huang H, Nicoli M, *et al.* A tutorial on 5G positioning. *arXiv* 2023, arXiv:2311.10551.

[11] Ajam H, Najafi M, Jamali V, Schmauss B, Schober R. Modeling and design of IRS-assisted multilink FSO systems. *IEEE Trans. Commun.* 2022, 70(5):3333–3349.

[12] Aboagye S, Ndjiongue AR, Ngatched TMN, Dobre OA, Poor HV. RIS-assisted visible light communication systems: a tutorial. *IEEE Commun. Surv. Tutorials* 2023, 25(1):251–288.

[13] Sun S, An N, Yang F, Song J, Han Z. Capacity characterization analysis of optical intelligent reflecting surface assisted MISO VLC. *IEEE Internet Things J.* 2024, 11(3):4801–4814.

[14] Di Renzo M, Ntontin K, Song J, Danufane FH, Qian X, *et al.* Reconfigurable intelligent surfaces *vs.*

relaying: differences, similarities, and performance comparison. *IEEE Open J. Commun. Soc.* 2020, 1:798–807.

[15] Ndjiongue AR, Dobre OA, Shin H. On-demand RIS-assisted free space optical access system for 6G networks. *IEEE Trans. Veh. Technol.* 2025, 74(6):9059–9070.

[16] Wang F, Lu M, Li X, Yang L, Mumtaz S, *et al.* Enhancing secrecy of indoor optical RIS aided SSK VLC downlink. *IEEE Trans. Wireless Commun.* 2025, 24(4):2783–2796.

[17] Sun Y, Wang F, Li R, Shi S, Li Y, *et al.* Joint SSK assisted by mirror array grouping and LEDs in indoor VLC system. *IEEE Trans. Veh. Technol.* 2025, 74(8):13139–13144.

[18] Abdelhady AM, Salem AKS, Amin O, Shihada B, Alouini MS. Visible light communications via intelligent reflecting surfaces: metasurfaces *vs.* mirror arrays. *IEEE Open J. Commun. Soc.* 2021, 2:1–20.

[19] Nasri A, Bafghi AHA, Nasiri-Kenari M. Wireless localization in the presence of intelligent reflecting surface. *IEEE Wireless Commun. Lett.* 2022, 11(7):1315–1319.

[20] Wang H, Zhang Z, Zhu B, Dang J, Wu L. Optical reconfigurable intelligent surfaces aided optical wireless communications: opportunities, challenges, and trends. *IEEE Wireless Commun.* 2023, 30(5):28–35.

[21] Wen Y, Yang F, Song J, Han Z. Optical integrated sensing and communication: architectures, potentials and challenges. *IEEE Internet Things Mag.* 2024, 7(4):68–74.

[22] Iddrisu I, Gezici S. Visible light positioning with intelligent reflecting surfaces under mismatched orientations. *Signal Process.* 2025, 230:109867.

[23] Sun S, Yang F, Song J. Sum rate maximization for intelligent reflecting surface-aided visible light communications. *IEEE Commun. Lett.* 2021, 25(11):3619–3623.

[24] Lu M, Wang F, Li R, Zuo T, Zhang J. Mirror array aided indoor SSK visible light downlink. *Opt. Commun.* 2023, 528:129004.

[25] Ma T, Xiao Y, Lei X, Xiong W, Xiao M. Distributed reconfigurable intelligent surfaces assisted indoor positioning. *IEEE Trans. Wireless Commun.* 2023, 22(1):47–58.

[26] Wang Y, Wu S, Yu L, Xu C, Wang Z, *et al.* RIS-assisted indoor visible light positioning based on sparse Bayesian learning. In *2023 3rd International Conference on Intelligent Communications and Computing (ICC)*, Nanchang, China, November 24–26, 2023, pp. 90–97.

[27] Guo Y, Wang F, Li R, Shi S, Li X, *et al.* Optical IRS assisted-visible light positioning in indoor non-LOS IoV scenarios. *IEEE Internet Things J.* 2025, 12(14):27686–27698.

[28] Dixit V, Kumar A, Sharan N, Pandey S, Kumar A, *et al.* Optimizing intelligent reflecting surface assisted visible light communication networks under blockage and practical constraints using TLBO for IoT applications. *Sci. Rep.* 2025, 15(1):27400.

[29] Siddiqi UF, Sait SM, Uysal M. Deep Q-learning based optimization of VLC systems with dynamic time-division multiplexing. *IEEE Access* 2020, 8:120375–120387.

[30] Jin J, Lu H, Wang J, Huang J, Feng L, *et al.* Adaptive feedback threshold based demodulation for mobile visible light communication and positioning integrated system. *Opt. Express* 2022, 30(8):13331.

[31] Ma S, Yang R, Du C, Li H, Wu Y, *et al.* Robust power allocation for integrated visible light

positioning and communication networks. *IEEE Trans. Commun.* 2023, 71(8):4764–4777.

[32] Di Renzo M, Zappone A, Debbah M, Alouini MS, Yuen C, *et al.* Smart radio environments empowered by reconfigurable intelligent surfaces: how it works, state of research, and the road ahead. *IEEE J. Sel. Areas Commun.* 2020, 38(11):2450–2525.

[33] Zuo T, Wang F, Zhang J. Sparsity signal detection for indoor GSSK-VLC system. *IEEE Trans. Veh. Technol.* 2021, 70(12):12975–12984.

[34] Liu Z, Yang F, Song J, Han Z. NOMA-based MISO visible light communication systems with optical intelligent reflecting surface: joint active and passive beamforming design. *IEEE Internet Things J.* 2024, 11(10):18753–18767.

[35] Maraqa O, Aboagye S, Ngatched TMN. Optical STAR-RIS-aided VLC systems: RSMA versus NOMA. *IEEE Open J. Commun. Soc.* 2024, 5:430–441.

[36] Sun S, Yang F, Song J, Han Z. Joint resource management for intelligent reflecting surface–aided visible light communications. *IEEE Trans. Wireless Commun.* 2022, 21(8):6508–6522.

[37] Ajam H, Najafi M, Jamali V, Schober R. Optical IRSs: power scaling law, optimal deployment, and comparison with relays. *IEEE Trans. Commun.* 2024, 72(2):954–970.

[38] Imani MF, Smith DR, del Hougne P. Perfect absorption in a disordered medium with programmable meta-atom inclusions. *arXiv* 2020, arXiv:2003.01766.

[39] Xu S, Wu Y, Wang X, Wei F. Indoor high precision positioning system based on visible light communication and location fingerprinting. *J. Lightwave Technol.* 2023, 41(17):5564–5576.

[40] Albanese A, Mursia P, Sciancalepore V, Costa-Perez X. PAPIR: practical RIS-aided localization via statistical user information. In *2021 IEEE 22nd International Workshop on Signal Processing Advances in Wireless Communications (SPAWC)*, Lucca, Italy, September 27–30, 2021, pp. 531–535.

[41] Association IS. IEEE standard for local and metropolitan area networks–part 15.7: short-range wireless optical communication using visible light. 2021. Available: https://ieeexplore.ieee.org/document/6016195 (accessed on 8 November 2025).

[42] Kahn J, Barry J. Wireless infrared communications. *Proc. IEEE* 1997, 85(2):265–298.

[43] Chow CW. Optical wireless communication-recent progresses and future perspectives. *J. Lightwave Technol.* 2025, pp. 1–15.

[44] Yoon S, Lee K, Cha J, Mariappan V, Young K, *et al.* IEEE Standard for Local and metropolitan area networks–Part 15.7: Short-Range Optical Wireless Communications. 2019. Available: https://ieeexplore.ieee.org/document/8697198 (accessed on 8 November 2025).

[45] Ma S, Cao S, Li H, Lu S, Yang T, *et al.* Waveform design and optimization for integrated visible light positioning and communication. *IEEE Trans. Commun.* 2023, 71(9):5392–5407.

[46] Wang TQ, Sekercioglu YA, Neild A, Armstrong J. Position accuracy of time-of-arrival based ranging using visible light with application in indoor localization systems. *J. Lightwave Technol.* 2013, 31(20):3302–3308.

[47] Keskin MF, Gezici S, Arikan O. Direct and two-step positioning in visible light systems. *IEEE Trans. Commun.* 2018, 66(1):239–254.